AN INVESTIGATION OF A METHOD OF AIRCRAFT CONTROL BY SHOCK WAVE INTERFERENCE

A THESIS

Presented to

the Faculty of the Graduate Division

by

Edward Cleveland Aldridge, Jr.

In Partial Fulfillment

of the Requirements for the Degree

Master of Science in Aeronautical Engineering

Georgia Institute of Technology

September, 1961

58
12R

AN INVESTIGATION OF A METHOD OF AIRCRAFT CONTROL BY SHOCK WAVE INTERFERENCE

Approved:

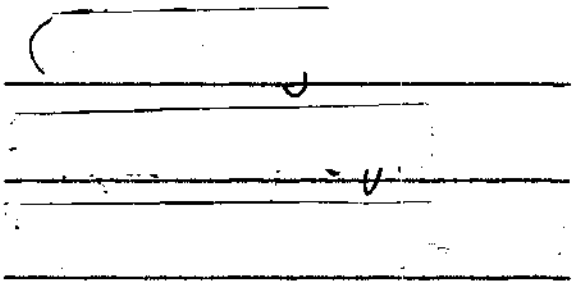

Date Approved by Chairman: October 25, 1961

"In presenting the dissertation as a partial fulfillment of the requirements for an advanced degree from the Georgia Institute of Technology, I agree that the Library of the Institution shall make it available for inspection and circulation in accordance with its regulations governing materials of this type. I agree that permission to copy from, or to publish from, this dissertation may be granted by the professor under whose direction it was written, or, in his absence, by the dean of the Graduate Division when such copying or publication is solely for scholarly purposes and does not involve potential financial gain. It is understood that any copying from, or publication of, this dissertation which involves potential financial gain will not be allowed without written permission.

_____

_____

ACKNOWLEDGMENTS

The author wishes to express his appreciation to Dr. Robin B. Gray for his assistance and invaluable comments throughout the preparation of this thesis.

Thanks are also extended to Dr. Frank M. White, Jr. and Professor Howard L. Durham for their review and criticism of this investigation.

The help and comments of the Aeronautical Engineering graduate students, along with the patience of Mrs. Judy Robinson in typing this work, are also appreciated.

TABLE OF CONTENTS

LIST OF FIGURES

Figure Page

LIST OF SYMBOLS

C_L	Lift coefficient, $\frac{\text{Lift}}{qS}$
c_l	Section lift coefficient
C_l	Rolling moment coefficient, $\frac{2(\text{Moment})}{q\ S\ b}$
C_p	Pressure coefficient, $\frac{P - P_l}{q}$
pb/2V	Rolling effectiveness
C_D	Drag coefficient, $\frac{\text{Drag}}{qS}$
C_{l_p}	Damping in roll coefficient, $\frac{\partial\, c_l}{\partial(pb/2V)}$
C_{l_δ}	Derivative of the rolling moment coefficient with respect to flap deflection angle, $\frac{\partial C_l}{\partial \delta}$
D	Drag, pounds
L	Rolling moment, foot-pounds, or subscript referring to losses, or subscript referring to lift
P	Rolling velocity, radians per second
S	Exposed wing plan form area, square feet
b	Exposed wing span, feet
V	Freestream velocity, feet per second
M	Freestream Mach number
M_2	Mach number behind the shock wave
AR	Aspect ratio, b^2/S
B_o	$\sqrt{M^2 - 1}$
B	$\sqrt{M_2^2 - 1}$
q	Freestream dynamic pressure, pounds per square foot
P	Pressure, pounds per square foot
P_l	Freestream pressure

A	Area, square feet
A'	Non-dimensional area, A/S
h	Fuselage flap height, feet
h'	Non-dimensional flap height, h/c
y	Spanwise distance, feet
y'	Non-dimensional spanwise distance, 2y/b
c	Wing root chord, feet
c_y	Wing chord at distance y along span, feet
a_o	Three-dimensional lift curve slope
te	Subscript referring to trailing edge
t	Subscript referring to total
s	Subscript referring to shock wave
I,II,III	Refers to regions I, II, or III on the wing surface
α	Ray angle in conical flow field
α_o	Angle of attack of the wing
Λ	Sweep angle
θ	Shock wave angle
μ_1	Mach angle, $\sin^{-1}(1/M)$
μ	Mach angle, $\sin^{-1}(1/M_2)$
γ	Ratio of specific heats, 1.4
δ	Flap extension angle

SUMMARY

Because of the increased speeds of today's aircraft, difficult aerodynamic and structural problems associated with control characteristics have created a need to find a new method of aircraft control at supersonic speeds. By assuming oblique shock theory, inviscid flow, a rigid body, steady state conditions, and a single degree of freedom, the rolling effectiveness and drag coefficient were determined theoretically for a fuselage flap control system based on the principle of shock wave interference.

The equation of motion for an aircraft in a steady roll was solved to give the rolling effectiveness:

$$\left(\frac{pb}{2V}\right)/\delta = -\frac{C_{l_\delta}}{C_{l_p}}$$

The expression C_{l_p} was found by using strip theory to be

$$C_{l_p} = -\frac{8a_o}{Sb^2}\int_0^{b/2} c_y y^2\, dy$$

where a_o is the linearized three-dimensional lift-curve slope.

The three-dimensional pressure losses were divided into three regions behind the shock wave. The pressure coefficient given by conical flow theory,

$$C_p = C_{p_s}\frac{\cos^{-1}}{\pi}(1 - 2B\tan\alpha),$$

was then integrated to give the rolling moment coefficient in each region; however, it was more convenient to find the loss in rolling moment coefficient in each region and subtract this value from the coefficient that would be obtained if there were no losses behind the shock. The rolling moment coefficient was then plotted as a function of the flap extension angle and the curve numerically differentiated to give C_{l_δ}. The ratio of C_{l_δ} and C_{l_p} then gave the desired rolling effectiveness which has been compared graphically with the rolling effectiveness for conventional control systems. The rolling effectiveness analysis was performed for a rectangular, a forty-five degree swept, and a delta wing.

The drag coefficient was obtained by summing the pressure forces determined from shock-expansion theory of the fuselage flap in the axial direction. The resulting coefficient was then graphically compared with experimental and theoretical drag coefficients for conventional control systems.

From the results of the rolling effectiveness analysis it was concluded that the fuselage flap control system is more effective than ailerons and wing tip ailerons as a method of rolling control for Mach numbers from 1.2 to 2.0 on a delta wing. The all-moveable wing was shown graphically to be much more effective in rolling than the fuselage flap except at Mach number 1.2 on the rectangular wing and Mach number 2.1 on a swept wing. For Mach numbers less than 2.1 the fuselage flap used in conjunction with a forty-five degree swept wing has been shown to be an excellent control device.

Results of the drag analysis indicate that the fuselage flap drag coefficient is comparable to all types of controls excepting wing tip

ailerons.

Viscous effects were neglected to limit the scope of this investigation. However, these effects could possibly be a major factor in the fuselage flap control characteristics. Further investigations should include the viscous effect. It is also recommended that a wind tunnel test be performed to study the aeroelastic problem and to substantiate the theoretical approach and date obtained in this study.

CHAPTER I

INTRODUCTION

As flight speeds of present day aircraft have been extended into the supersonic regime, aerodynamic and structural problems associated with conventional control systems have become increasingly acute. The high velocities encountered and the types of control employed have resulted in a considerable weight penalty from the structural stiffening required to counteract the aeroelastic effect arising from unfavorable load concentrations. Thin-winged aircraft pay hazardous penalties in control effectiveness as a result of this aeroelastic effect. Some solutions to the structural problem incorporate all-moveable wings and tails and wing tip ailerons, but the problem still exists because of the load concentration at the control axis. According to Stone[1*], spoilers have been proposed because of the decrease in twisting moment compared with the aileron, but since large drag forces are created by spoilers at high speeds, other types of control may be more advantageous. Blowing jets have been investigated by Schult[2] for use as a control device to relieve the structural problem, but they were shown to be less effective and to have higher drag than all moveable wings, plain flaps, or spoilers. Reaction-type controls have been investigated by Hunter[3], but their applicability lies only with missiles which require no roll control.

Illustrations of the aeroelastic problem including the effect of

---

*Superscripts refer to items in Bibliography.

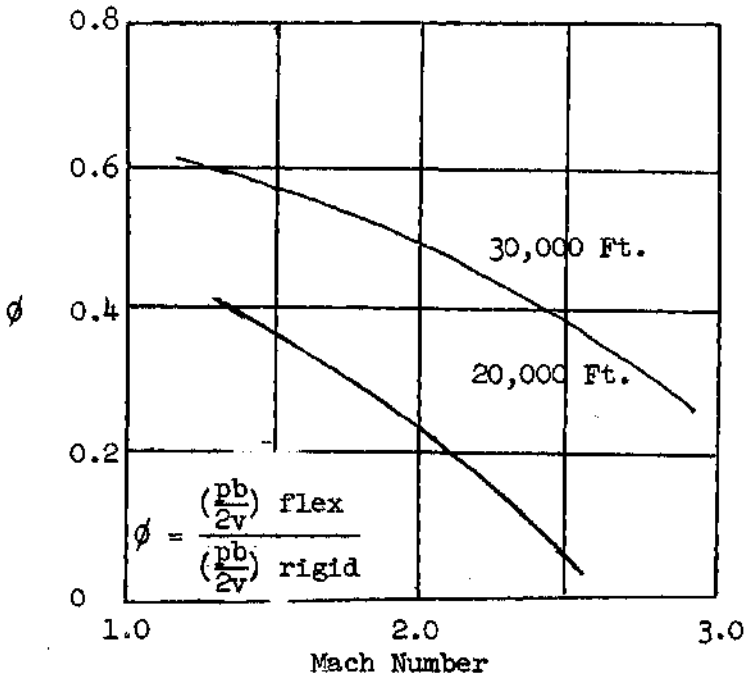

Data For:
Flat Plate 0.02 C Thick, Full Span Ailerons, of Chord 0.2 C, and an Aspect Ratio of 1.5

Fig. 1 Aeroelastic Effect Due to Aileron Deflection for a Rectangular Flat Plate Wing. (Ref. 4)

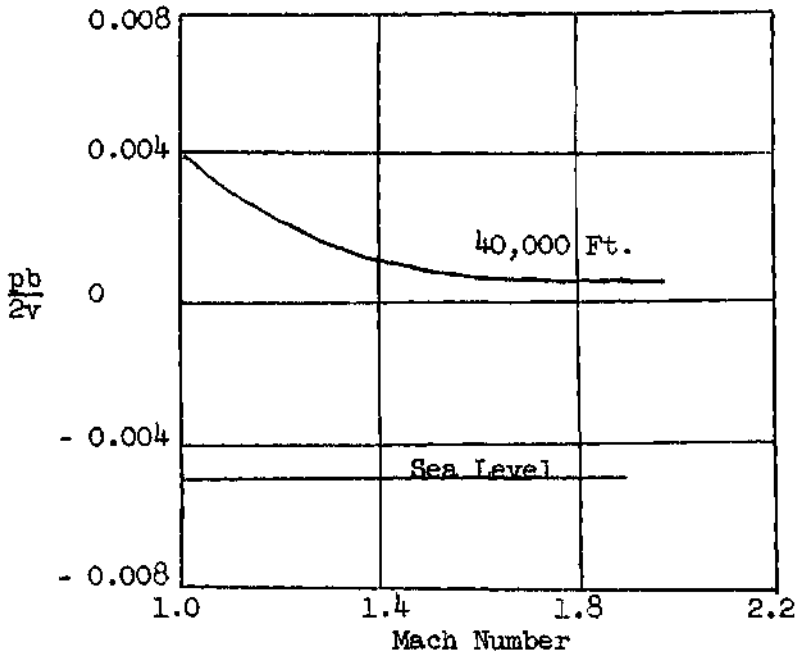

Data For:
65A006 Airfoil, Aspect Ratio of 4.0, Full Span Ailerons of 0.3 C, and a Taper Ratio of 0.6

Fig. 2 Aeroelastic Effect Due to Aileron Deflection for a Forty-Five Degree Swept Wing. (Ref. 1)

altitude, are shown in Fig. 1, from Hedgepeth and Kell[4], and Fig. 2, from Stone[1], where the rolling effectiveness is plotted as a function of Mach number. These two figures illustrate the problem facing aircraft engineers in the design of aircraft control systems. Figure 1 shows the effect of aeroelasticity on an aileron system with altitude and with increasing Mach number. At the higher Mach number and lower altitude, the rolling effectiveness approaches negative values, or the aileron reaches its reversal speed. Figure 2 shows the effect of altitude on the rolling effectiveness of a flexible wing. With increasing Mach number the rolling effectiveness at 40,000 feet decreases, approaching a limiting value, but at sea level, the aileron has reached its reversal speed before the sonic Mach number.

Another problem which must be considered is the weight penalty resulting from the use of heavy, high-pressure hydraulic control systems required to activate the control devices at high speeds. The use of all moveable wings and tails and wing-tip ailerons have eliminated the problem of large control forces, but the structural weight required to accommodate the loads at the control axis cancels the advantage gained from a light-weight control mechanism.

Because of these problems there exists a need to consider new methods of aircraft control at supersonic speeds. The following presentation is an investigation of a new aircraft or winged missile control system based on the principle of shock wave interference in which the pressure rise associated with the shock wave is directed on an aircraft or missile component to generate a control force.

Eggers and Syvertson[5] investigated the principle of shock wave in-

terference as applied to maximum lift-drag ratios obtained by arranging aircraft components in such a way as to utilize the fuselage bow shock. The feasibility of this principle for use as a method of control is confirmed by noting that Eggers and Syvertson obtained experimental lift-drag ratios of the order of six and greater.

Holder and Lock[6] have investigated the use of a fuselage flap as a lateral control device with the assumption of linearized first order theory. Their results indicated that a more refined theoretical analysis should be performed, making use of oblique shock relations to develop the rolling effectiveness and the drag of such a control system.

The purpose of this presentation is to develop the relations for the rolling effectiveness and drag of the fuselage flap control system under consideration. The values obtained from these relations will then be compared with those for control systems now in use for a rectangular, a forty-five degree swept, and a delta wing.

CHAPTER II

CONFIGURATION AND ASSUMPTIONS

The new control system under consideration consists basically of a flap located on the side of the fuselage at the wing or tail of the aircraft which could be extended or retracted on command for the purpose of maneuver or flight path correction. Upon extension at supersonic speeds the flow turned by the flap creates a shock wave which passes over the wing or tail surface. The ambient pressure rise associated with the shock wave acts on the area behind the shock front, resulting in a rolling, pitching, or yawing moment about the center of gravity (see Fig. 3). A similar control force can be created by retracting a flap into the fuselage, causing a decrease in ambient pressure due to expansion. For the purpose of simplification only the extended flap for lateral control will be investigated here.

To obtain an order of magnitude of the control forces created by the fuselage flap control, a wedge type body was assumed for this presentation. The wedge has a maximum thickness at a distance equal to the wing root chord and the wedge leading edge is at the wing leading edge (see Fig. 4). For a swept wing the flap must be extended beyond the root chord so that the expansion wave from the vertex will not reduce the pressure on the wing surface. For small extension angles, however, this increase in length can be neglected.

There are several advantages which the fuselage flap system has over conventional control systems. Since the center of pressure for such a system moves inboard and forward, the twisting moment on the wing is

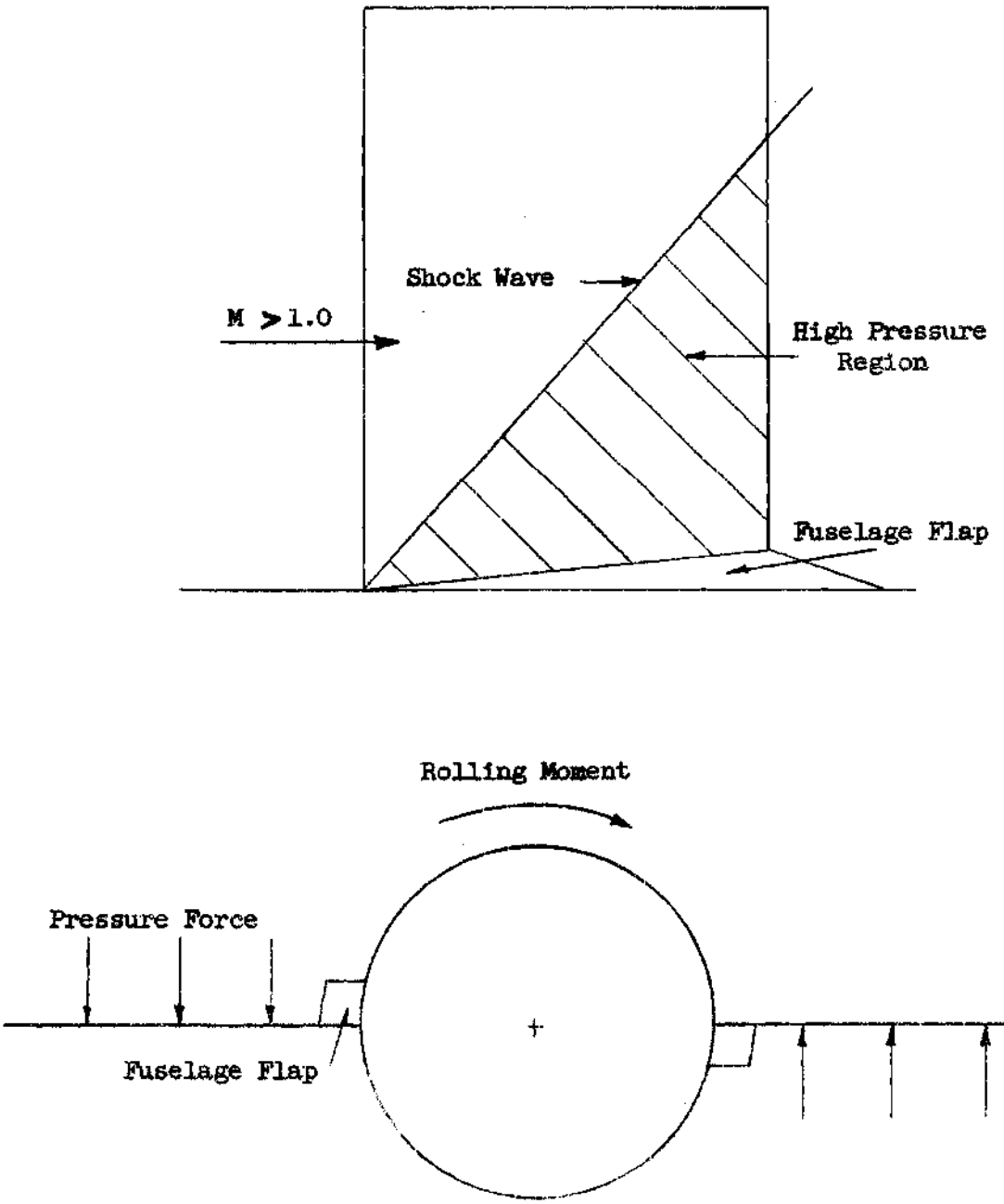

Fig. 3 Rolling Control Force Created By Extension of Fuselage Flap.

reduced. Hence, less structural stiffening is required than for conventional aileron controls. Large load concentrations are not a factor here as in the case of all-moveable wings where large forces are found at the wing axis. Also, a control mechanism which converts forces to torque is not required since the fuselage flap could be extended by a light-weight pushing mechanism inside the fuselage. This would reduce the weight of the conventional control system since it would not be used at supersonic speeds where, excepting all-moveable controls, large control forces are required.

There are several simplifying assumptions which must be made in order that a preliminary investigation, such as this presentation, can be carried out. The most important of these assumptions is the neglect of viscous effects. One of the difficulties arising when viscosity influences the flow occurs when the shock wave from the fuselage flap impinges on the wing boundary layer. Little is known about how this impingement influences the drag. Also, as a result of viscosity, there will be a spanwise flow component due to the pressure gradient in the boundary layer which causes flow out of the high pressure region behind the shock front to the lower pressure region forward of the shock, or, as in Fig. 5, from point (2) to point (1). In order to limit the scope of this presentation the effect of viscosity will be neglected.

Another spanwise component of the flow comes about as a result of turning the flow by the extension of a control flap. Since flap deflections will be limited to angles between two and ten degrees, this spanwise component is small and will be assumed to have no influence on the control characteristics.

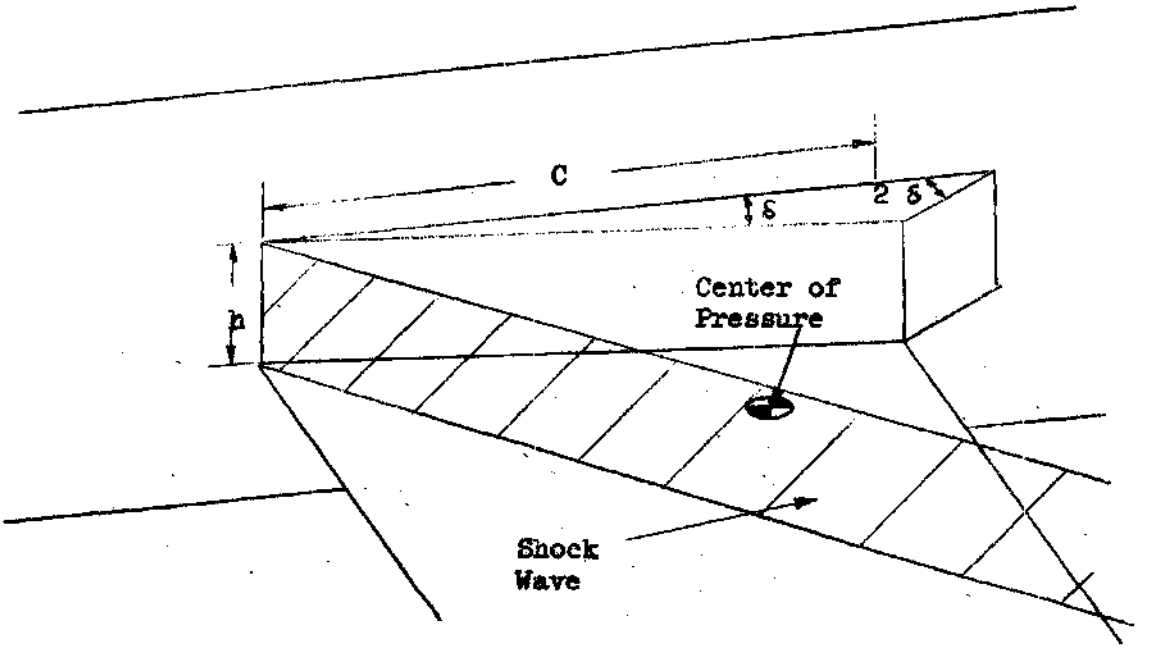

Fig. 4 Fuselage Flap Configuration Used to Develop the Control Force

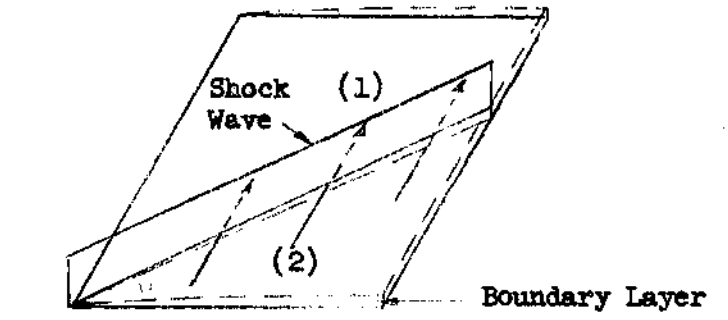

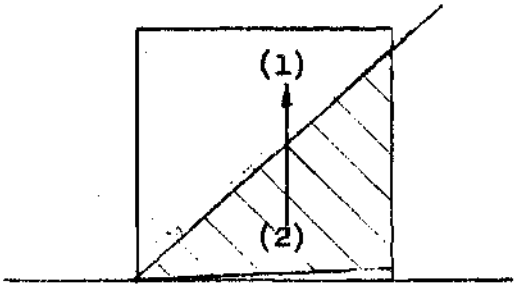

Fig. 5 Spanwise Flow as a Result of the Pressure Gradient in the Boundary Layer on the Wing

It must also be assumed that the shock wave from the lateral control flap lies behind the wing leading edge. This assumption is made in order to avoid the effect of the shock wave on the pressure of the wing under-surface which would cancel most of the desired control force.

To eliminate the consideration of aeroelastic and inertia effects the wing is assumed to be a rigid flat plate at zero angle of attack in a steady roll with a single degree of freedom. The assumptions of a single degree of freedom and a steady roll are not exact, but they eliminate cross-coupling effects and permit the equation of motion to be easily solved. The rigidity assumption is nec essary because the wing used here is arbitrary, and its properties must be known in order to solve the aeroelastic problem.

Since a constant pressure coefficient is desired behind the shock wave along its length, it must be shown that the shock wave is straight on the wing surface. Also, since the Mach angle at any point must be based on the local Mach number, the Mach angle on the wing surface must be based on the Mach number behind the shock wave. In most instances the shock angle is less than the wing surface Mach angle. Therefore, to have a straight shock wave it must be shown that the Mach waves from points of disturbance do not intersect the shock wave within the semi-span. It is assumed that there is no discontinuity in the flow except the shock wave. Hence, the Mach angle must change gradually from that of freestream above the shock front to that on the wing surface thereby producing the disturbance cone as seen in Fig. 6. Section A-A is the plane of intersection of the cone of disturbance with the wing surface. It can be seen that the angle along the line of intersection approaches the freestream Mach angle.

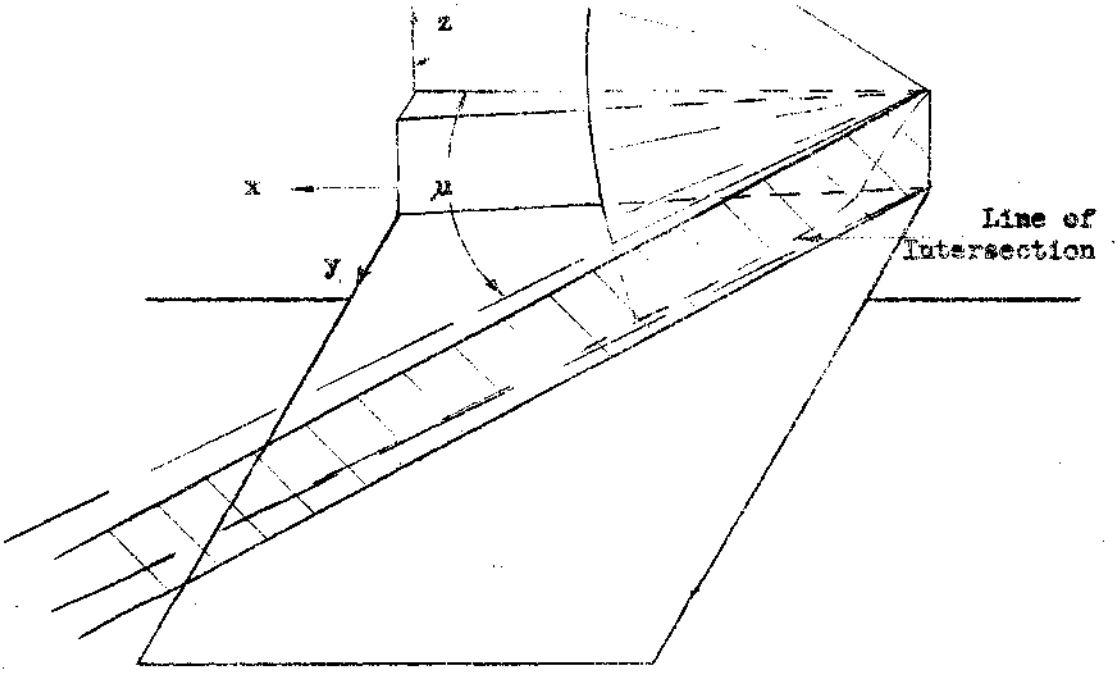

Views of Disturbance Cone

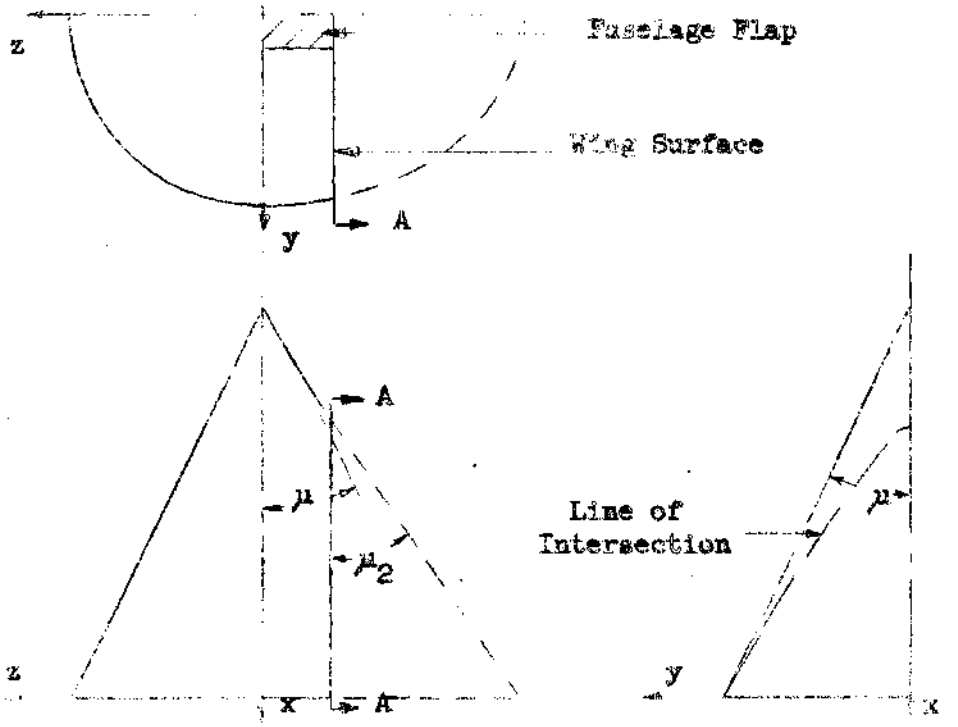

Fig. 6 Configuration of the Disturbance Cone from the Top of the Shock Front

asymptotically. Therefore, since the freestream Mach angle is less than the shock angle from second order theory, no intersection occurs.

A curved shock wave can also result if the expansion wave from the rear of the fuselage flap intersects the shock wave, however this does not occur for the wing aspect ratios under consideration as has been shown in Appendix I. Also, it is assumed that the shock wave strength does not deteriorate in the vicinity of the wing. Under these assumptions the shock wave used in this presentation is straight and the pressure coefficient is constant along its length. The wing is assumed to be attached to an infinite fuselage so that there are no effects on the wing or on the fuselage flap shock wave from the fuselage bow shock wave.

Finally, the gas is assumed to be perfect with a ratio of specific heats of 1.4.

Summarizing, the major assumptions made are:

1. Viscous effects are neglected,
2. Spanwise flow is neglected,
3. The wing is a rigid flat plate at zero angle of attack in a steady roll with a single degree of freedom,
4. The shock wave over the wing surface is straight,
5. Perfect gas, $\gamma = 1.4$.

Other less critical assumptions are to be found throughout the text of this investigation.

CHAPTER III

ROLLING EFFECTIVENESS

The rolling effectiveness will be found from the parameters C_{l_δ}, the change in rolling moment coefficient per change in flap deflection angle, and C_{l_p}, the change in rolling moment coefficient per change in wing tip helix angle, usually called the damping in rolling coefficient. The ratio of these derivatives will give the desired effectiveness parameter, the wing tip helix angle per degree of flap deflection. The derivation of the effectiveness parameter was obtained from Perkins and Hage[7] where, by summing moments about the aircraft centerline, the equation of motion for a roll is

$$I\dot{p} = \frac{\partial L}{\partial p} \cdot dp + \frac{\partial L}{\partial \delta} \cdot d \qquad (3.1)$$

where I is the moment of inertia about the fuselage centerline. For a flat plate at zero angle of attack $dp = p$ and $d\delta = \delta$, and in a steady roll Equation (3.1) can be written

$$0 = \frac{\partial L}{\partial p} \cdot p + \frac{\partial L}{\partial \delta} \cdot \delta$$

which becomes

$$p = - \frac{\left(\frac{\partial L}{\partial \delta}\right)}{\left(\frac{\partial L}{\partial p}\right)} \cdot \delta \qquad (3.2)$$

or, in coefficient form

$$\left(\frac{pb}{2V}\right)/\delta = -\frac{\frac{\partial C_l}{\partial \delta}}{\frac{\partial C_l}{\partial\left(\frac{pb}{2V}\right)}} = -\frac{C_{l\delta}}{C_{l_p}} \tag{3.3}$$

The damping in roll coefficient, C_{l_p}, can be found using strip theory. With regard to Fig. 7, the angle of attack, in radians, of any section due to the rolling velocity, p, can be approximated for small angles by

$$\alpha_o = \frac{p \cdot y}{V} \tag{3.4}$$

Hence, the section life coefficient, based on section area, for a flat plate due to rolling is

$$c_\ell = a_o \Delta\alpha_0 = a_o \frac{p \cdot y}{V} \tag{3.5}$$

The differential rolling moment coefficient can be expressed as

$$dC_l = \frac{c_\ell A_y y}{S\, b/2} = c_\ell \frac{A_y y}{Sb/2} \tag{3.6}$$

where A_y is the section area. Substitution of Equation (3.5) into Equation (3.6) then yields for the rolling moment coefficient

$$C_l = -\frac{4a_o p}{S\, b\, V}\int_0^{b/2} c_y y^2 dy \tag{3.7}$$

A negative sign is associated with Equation (3.7) since an increase in rolling velocity tends to decrease the rolling moment. Differentiating Equation (3.7) gives

$$C_{l_p} = \frac{\partial C_l}{\partial \left(\frac{pb}{2V}\right)} = -\frac{8a_o}{Sb^2} \int_0^{b/2} c_y y^2 \, dy \qquad (3.8)$$

In Appendix II it is shown that the three-dimensional lift curve slope, a_o, for a forty-five degree swept wing with a taper ratio of one, is approximated by

$$a_o = \frac{4}{B_o} \left[1 - \frac{1}{AR}\left(1 - \frac{2B_o - 1}{\sqrt{(2B_o + 1)^2 - 1}}\right) \right]; \qquad (3.9)$$

for a rectangular wing by

$$a_o = \frac{4}{B_o} \left[1 - \frac{1}{2 B_o AR} \right]; \qquad (3.10)$$

and for a delta wing by

$$a_o = \frac{4}{B_o} \qquad (3.11)$$

where $\frac{4}{B_o}$ is the linearized supersonic life curve slope given by Ackert Theory. Linearized theory is used here since it gives satisfactory results without complicated calulations to determine the pressure distribution on the wing surface.

The damping in roll coefficient is found by integrating Equation (3.8). For a taper ratio of one, Equation (3.8) becomes

$$C_{l_p} = -\frac{a_o}{3} \tag{3.12}$$

where a_o is dependent upon the type of wing in question, rectangular or swept. For a taper ratio of zero, corresponding to a delta wing, Equation (3.8) becomes

$$C_{l_p} = -\frac{2}{3B_o} \tag{3.13}$$

The plots of the damping in roll coefficient versus Mach number are found in Fig. 8 for a rectangular, a forty-five degree swept, and a delta wing, respectively.

The term, C_{l_δ}, the change in rolling moment coefficient due to a change in flap deflection, from Equation (3.4), was determined by solving for the rolling moment coefficient as a function of the flap deflection angle, plotting these values, and differentiating the curve.

The total rolling moment coefficient was found by subtracting the losses in rolling moment due to three-dimensional effects from the coefficient which would be obtained if a constant pressure existed on the wing behind the shock wave. The largest loss occurs as a result of the freestream conditions directly above the shock wave influencing the pressure distribution on the wing surface behind the shock (see Fig. 9). The loss in region I was found by integrating the product of the pressure coefficient, the incremental area, and the moment arm from the root chord of the wing and subtracting this value from the rolling moment coefficient obtained if the pressure were constant throughout the affected area on the wing surface. By assuming a conical flow field, the equation for the loss

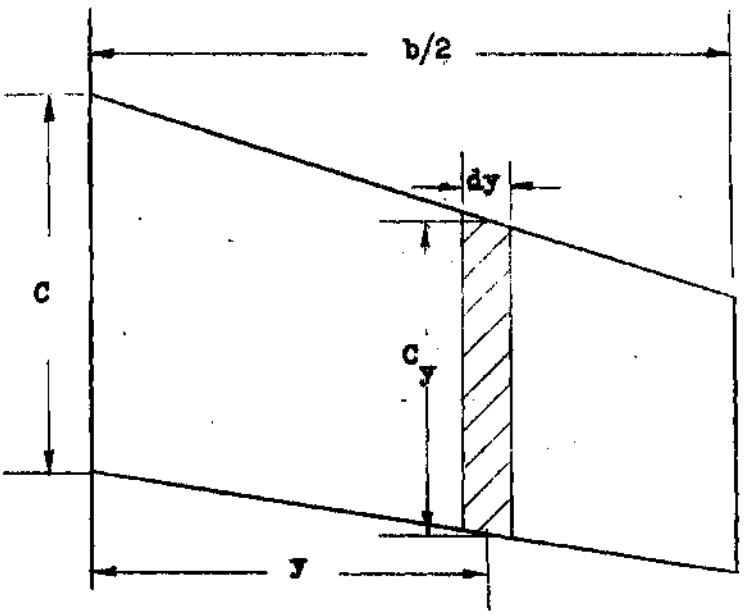

Fig. 7 An Arbitrary Wing used with Strip Theory in Determining the Damping in Roll Coefficient

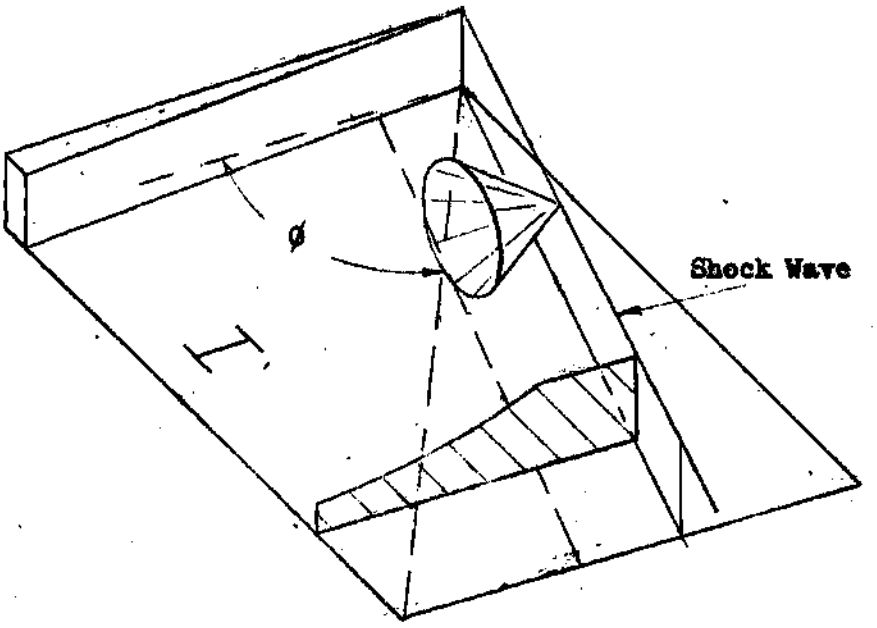

Fig. 9 Pressure Loss due to the Influence of Freestream Conditions Directly Above the Shock Front

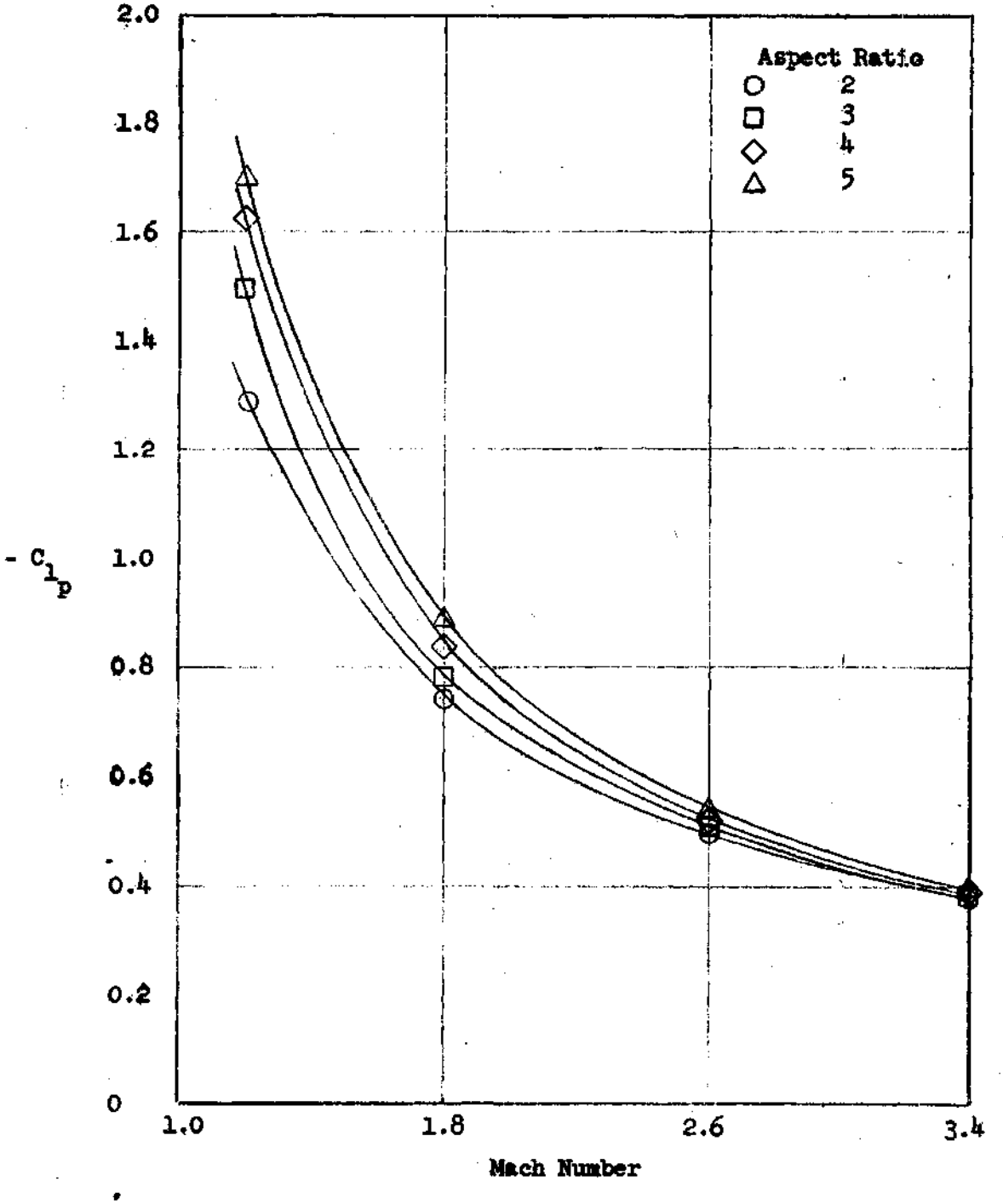

Fig. 8 Damping in Rolling Coefficient as a Function of Mach Number for Various Aspect Ratios. Rectangular Wing.

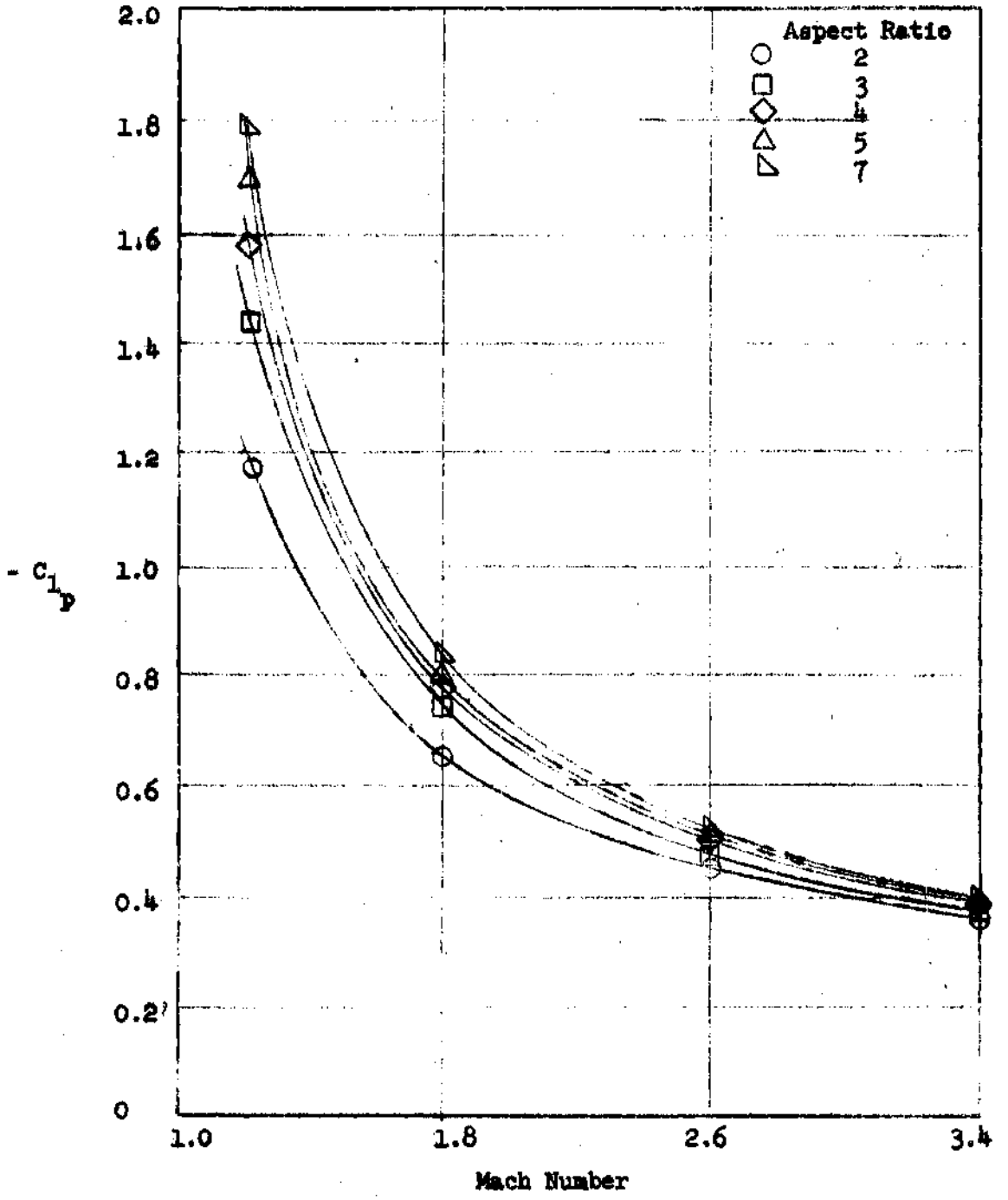

Fig. 8 (Continued) 45° Swept Wing

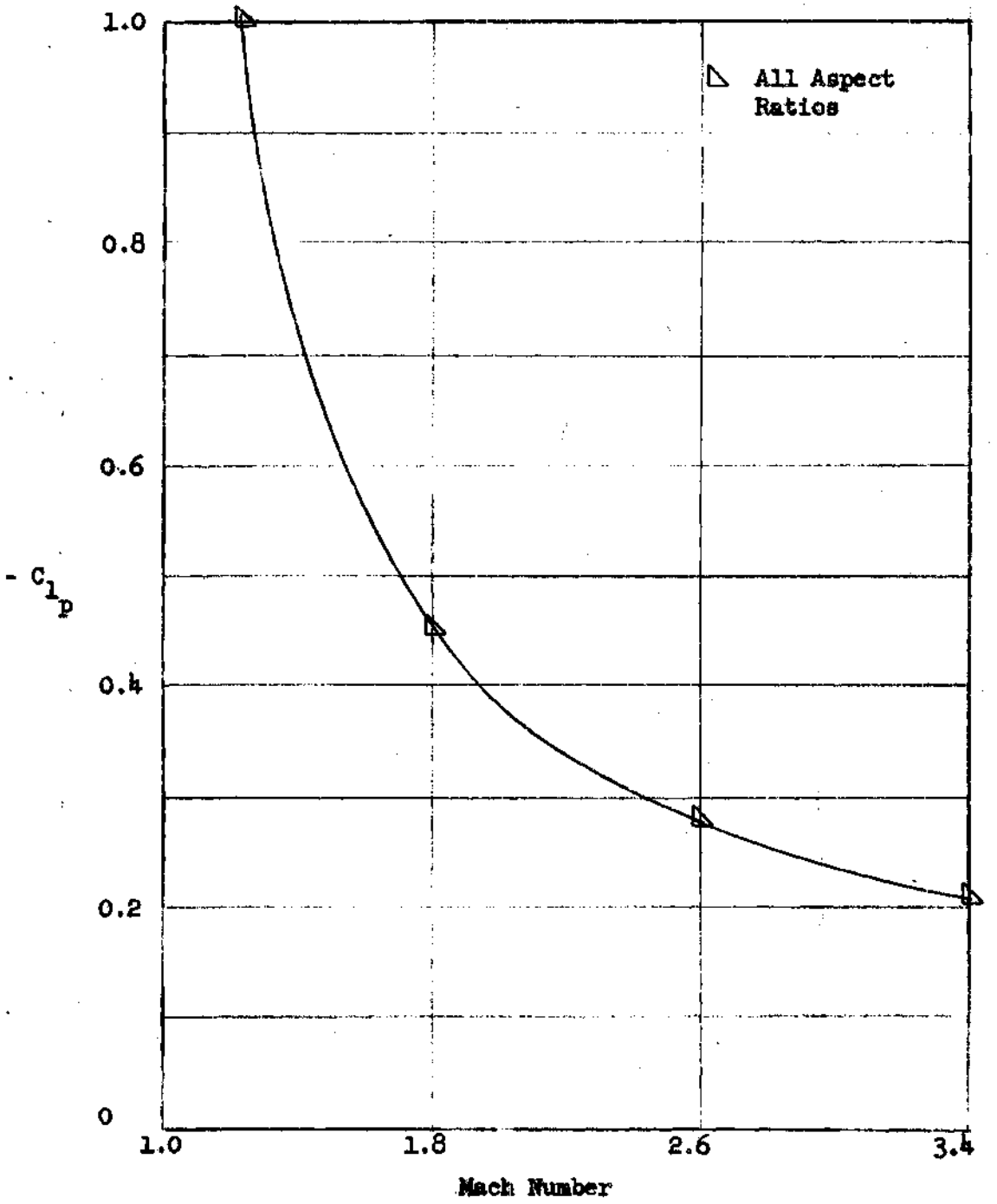

Fig. 8 (Concluded) Delta Wing

in rolling moment coefficient in region I has been found in Appendix III to be

$$C_{l_{L_I}} = C_{l_{S_I}} - C_{l_I} \tag{3.14}$$

where,

$$C_{l_{S_I}} = C_{p_s} \cdot \frac{A_I}{S} \cdot \frac{2\bar{y}}{b}$$

and

$$C_{l_I} = \frac{C_p h'B_1}{2} \int_0^{y^*} \left[\frac{1 - ty'}{h'B} \cos^{-1}\left(1 - \frac{2h'B}{1 - ty'}\right) + 2\sqrt{\frac{1 - ty'}{h'B} - 1} - \pi \right] y'dy'$$

where y^* , A_I , and $\bar{y}$ are dependent upon the shock angle, flap height, and Mach number (see Appendix III). It should be noted here that the Mach angle used in determining the areas of the regions behind the shock was based on the Mach number behind the shock, as seen by the use of B.

The second loss occurs if the shock wave intersects the wing tip. There is a loss in pressure behind the Mach cone from the intersection due to the freestream conditions outside the wing tip influencing the flow on the wing behind the Mach cone (see Fig. 10). As before, the loss in rolling moment coefficient in region II was found to be

$$C_{l_{L_{II}}} = C_{l_{s_{II}}} - C_{l_{II}} \tag{3.15}$$

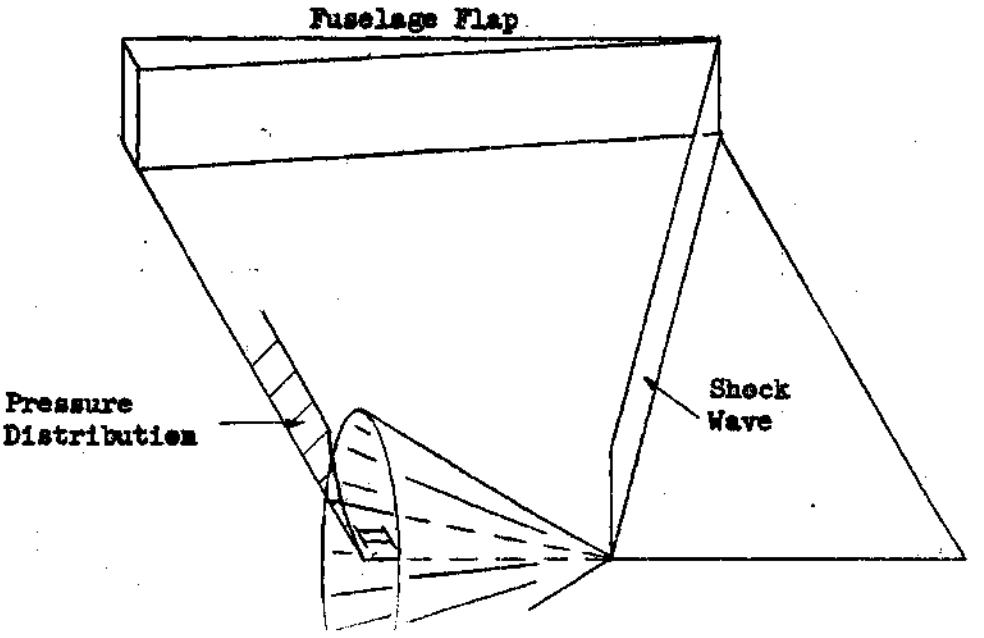

Fig. 10 Pressure Loss due to Tip Effect Behind the Shock Wave

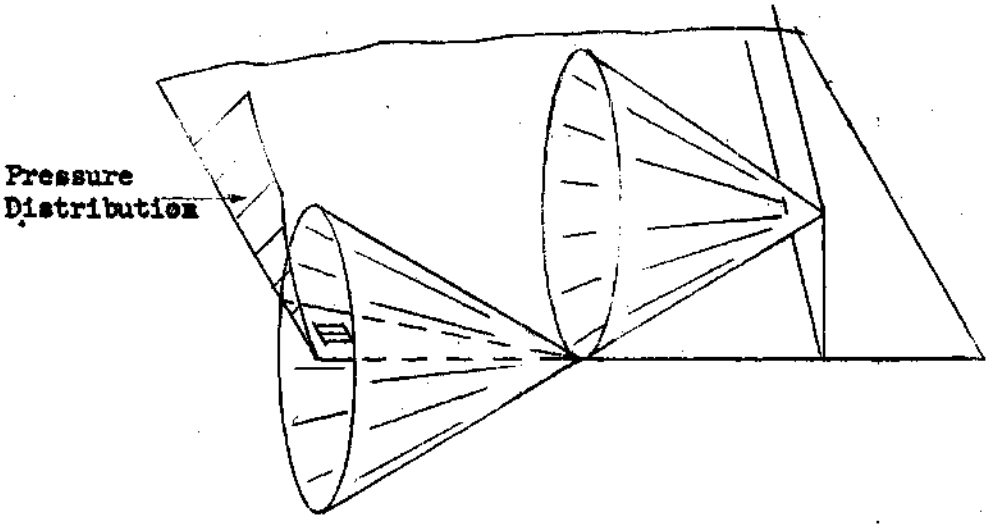

Fig. 11 Pressure Loss due to Tip Effect from the Intersection of the Mach Cone from the Shock Front and the Wing Tip

where

$$C_{l_{s_{II}}} = C_{P_s} \frac{\left(1 - \frac{AR.T}{2}\right)^2}{2.AR.(\tan \Lambda_{te} + B)} \left[1 - \frac{2\left(1 - \frac{AR.T}{2}\right)}{3.AR.(\tan \Lambda_{te} + B)}\right]$$

$$C_{l_{II}} = C_{P_s} \frac{\left(1 - \frac{AR.T}{2}\right)^2}{2\pi AR} \int_0^{\mu} \frac{\cos^{-1}(1 - 2B \tan \alpha)}{(\sin \alpha \tan \Lambda_{te} + \cos \alpha)^2} \left[1 - \frac{4\left(1 - \frac{AR.T}{2}\right)\sin \alpha}{3\ AR}\right] d\alpha$$

and,

$$T = \frac{1 - \tan \Lambda_{te} \tan \theta}{\tan \theta}$$

The final loss in rolling moment occurs when the Mach cone from the top of the shock fron intersects the wing tip (see Fig. 11). The flow outside the wing tip can influence the flow on the wing tip behind the Mach cone from the point of intersection. Conical flow theory no longer holds in region III since the pressure coefficient is influenced by the pressure coefficient in region II and is not constant along a ray from the Mach cone vertex; however, for simplification the flow in region III was assumed conical. Normally, the pressure coefficient along a Mach line is equal to the shock wave pressure coefficient, as in region II. In region III the pressure coefficient will not reach the shock wave value as a result of region II, therefore it was assumed that the pressure coefficient along the Mach line bordering region III was the average coefficient in

region II, or one-half of the shock wave pressure coefficient. The justification of this assumption is shown in Appendix IV.

The solution of the loss in rolling moment coefficient in region III was found to be

$$C_{l_{L_{III}}} = C_{l_{s_{III}}} - C_{l_{III}} \tag{3.16}$$

where

$$C_{l_{s_{III}}} = C_{P_s} \frac{(1 - \frac{AR.T}{2} - h'B)^2}{4.AR.(\tan \Lambda_{te} + B)} \left[1 - \frac{2(1 - \frac{AR.T}{2} - h'B)}{3\ AR.(\tan \Lambda_{te} + B)} \right]$$

and

$$C_{l_{III}} = C_{P_s} \frac{(1 - \frac{AR.T}{2} - h'B)^2}{4\pi\ .\ AR} \int_0^{\mu} \left\{ \frac{\cos^{-1}(1 - 2\ B \tan \alpha)}{(\sin \alpha \tan \Lambda_{te} + \cos \alpha)^2} \left[1 - \frac{4(1 - \frac{AR.T}{2} - h'B) \sin \alpha}{3.AR.(\sin \alpha \tan \Lambda_{te} + \cos \alpha)} \right] \right\} d\alpha$$

Since the linearized potential equation was used to determine the variation in pressure coefficient (see Equation (A.2)) in a disturbed region it follows that when any region intersects another, the losses arising in each can be linearly super-imposed.

The total rolling moment coefficient was found by determining the rolling moment coefficient that would occur if the pressure were constant in region S, the total area behind the shock, and subtracting the losses

from this value. The rolling moment coefficient for the shock wave greater than ϕ is

$$C_{l_s} = C_{p_s} \cdot \frac{(3 - AR.T)}{12}$$

where ϕ is the angle at which the shock wave begins to intersect the wing tip (see Fig. 9). The angle ϕ is determined for an arbitrary wing to be

$$\phi = \tan^{-1}\left[\frac{AR}{\frac{2(1 + AR.\tan\Lambda_{te})}{2}}\right]$$

The rolling moment coefficient for the shock wave angle less than ϕ becomes

$$C_{l_s} = \frac{C_{p_s}}{3.AR^2T^2}$$

Finally, the total rolling moment coefficient is given by

$$C_{l_t} = C_{l_s} - \sum C_{l_L}$$

where $\sum C_{l_L}$ is the sum of the losses in rolling moment coefficient due to outside influences.

The equations for the total rolling moment coefficient were solved on the Burroughs Datatron 220 Digital Computer. These values were plotted as a function of the flap deflection angle and flap height in Figs. 12 through 14 for a rectangular, a forty-five degree swept, and a delta wing,

Page missing from thesis

derivatives are obtained as those for a rectangular wing. It should be noted that there are no values plotted for the rolling moment coefficient parameter at a Mach number of 1.2 (see Fig. 14). At a Mach number of 1.2 a small flap extension causes a large shock wave angle, but it was assumed that the shock must lie behind the wing leading edge, hence, as the shock wave lies in front of the wing leading edge, this Mach number was not considered.

As in the case for a rectangular wing, the fuselage flap used with a delta wing affords good roll control for small aspect ratios and Mach numbers (see Fig. 17). At the larger Mach numbers, where the shock angle from the fuselage flap is small, there is an advantage in the large length of the moment arm to the center of pressure of ailerons and all-moveable wings.

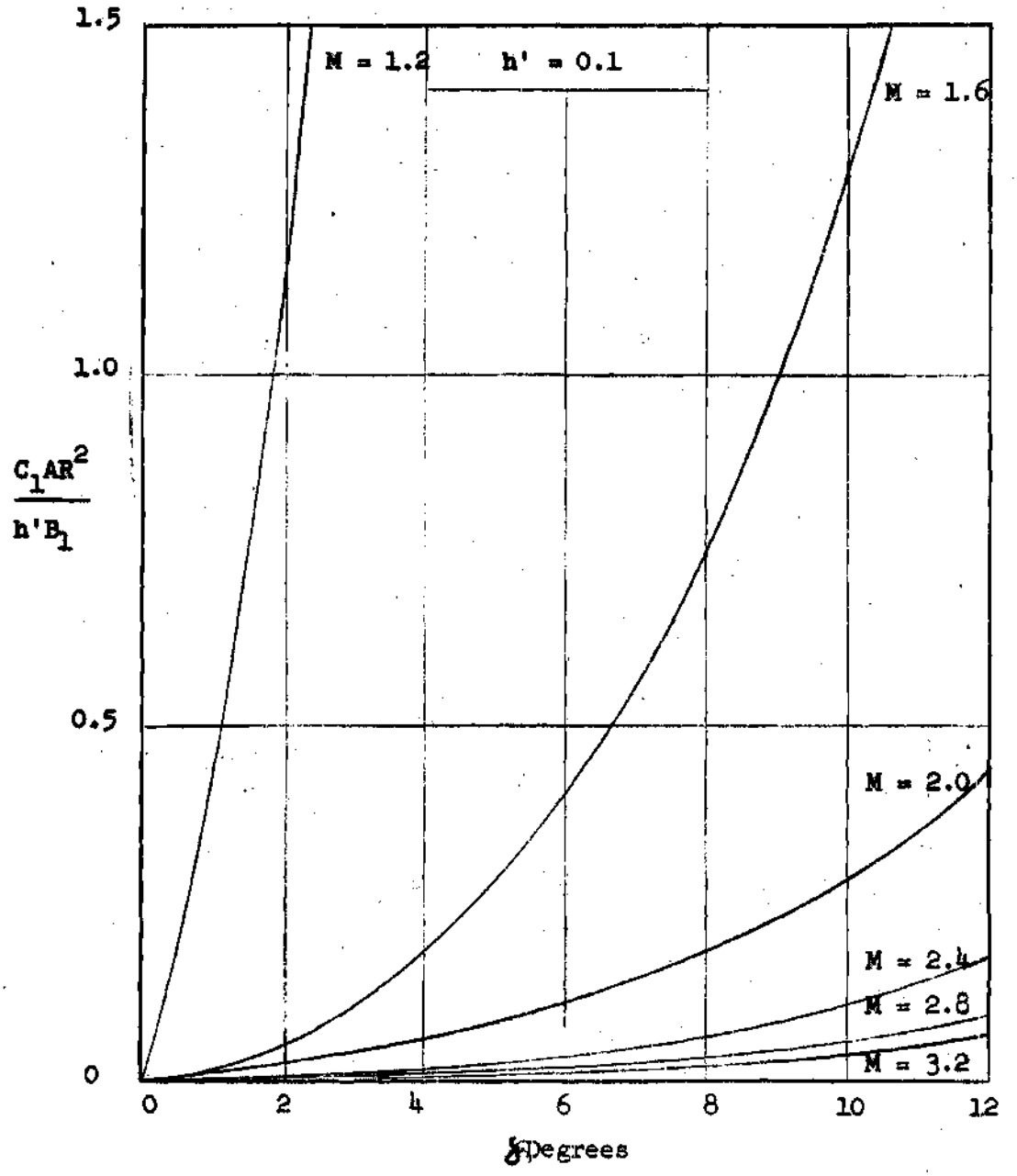

Fig. 12 Rolling Moment Coefficient for a Rectangular Wing as a Function of Flap Extension Angle for Various Mach Numbers

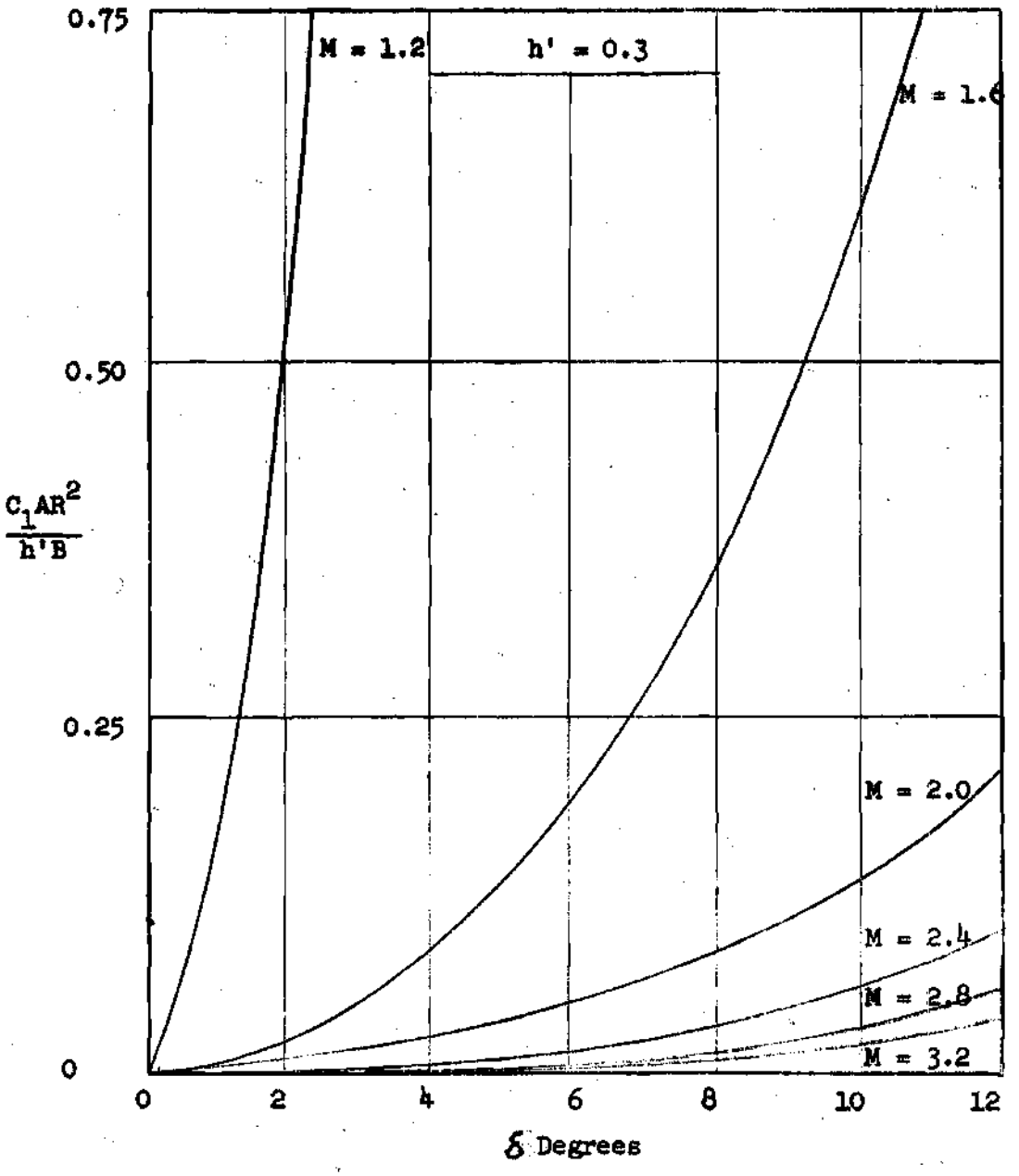

Fig. 12 (Concluded)

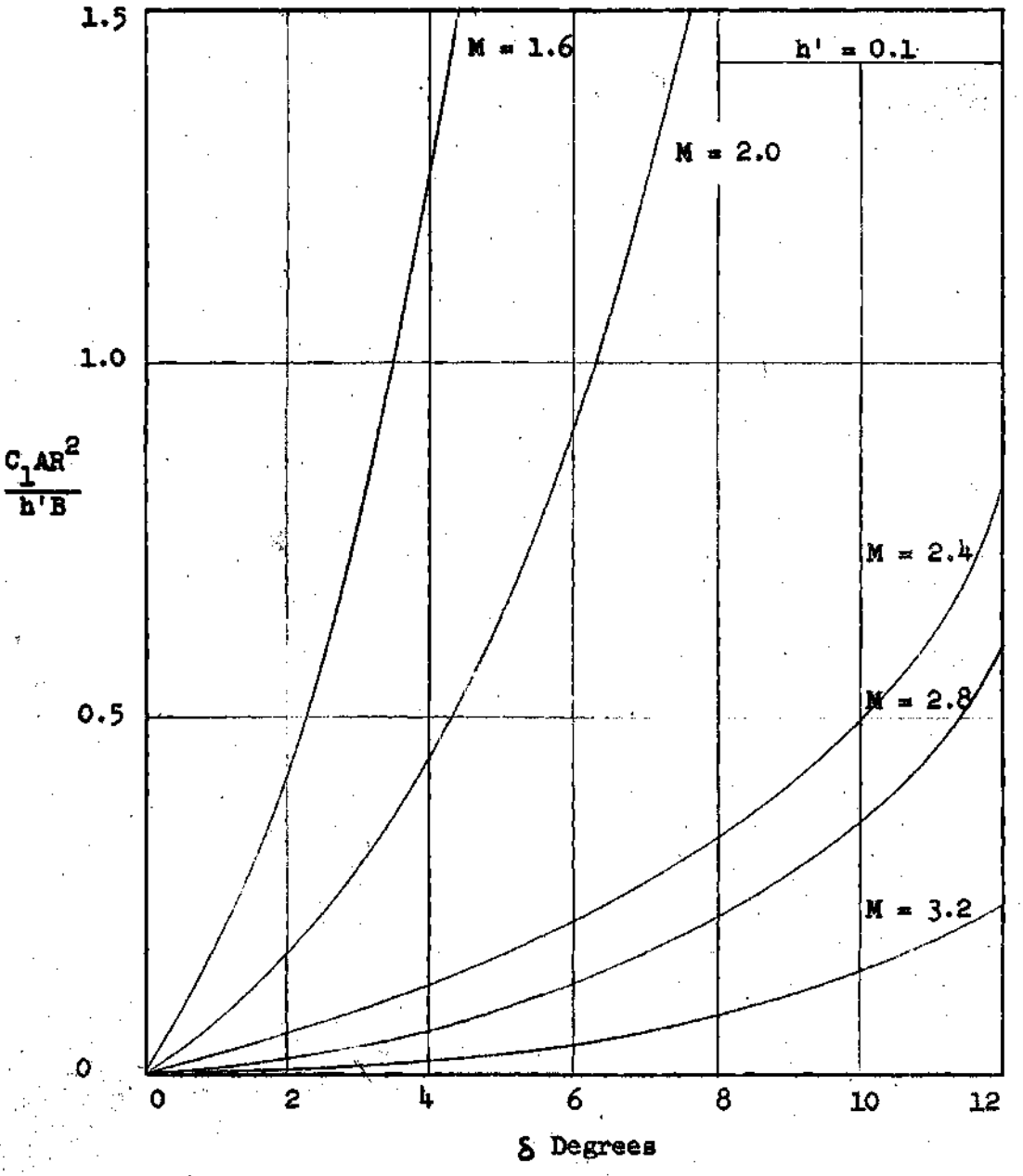

Fig. 13 Rolling Moment Coefficient for a Forty-Five Degree Swept Wing as a Function of the Flap Extension Angle for Various Mach Numbers

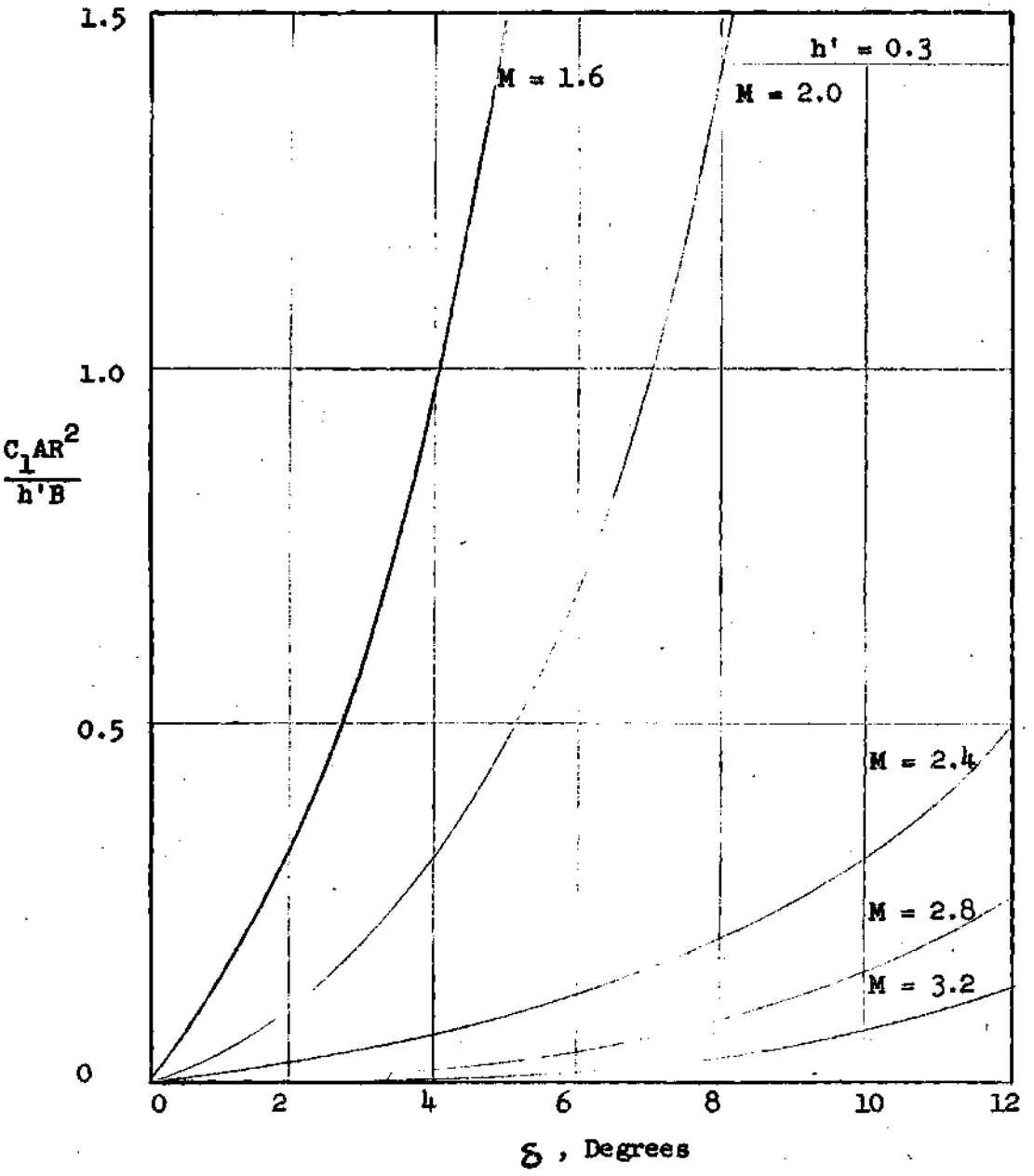

Fig. 13 (Concluded)

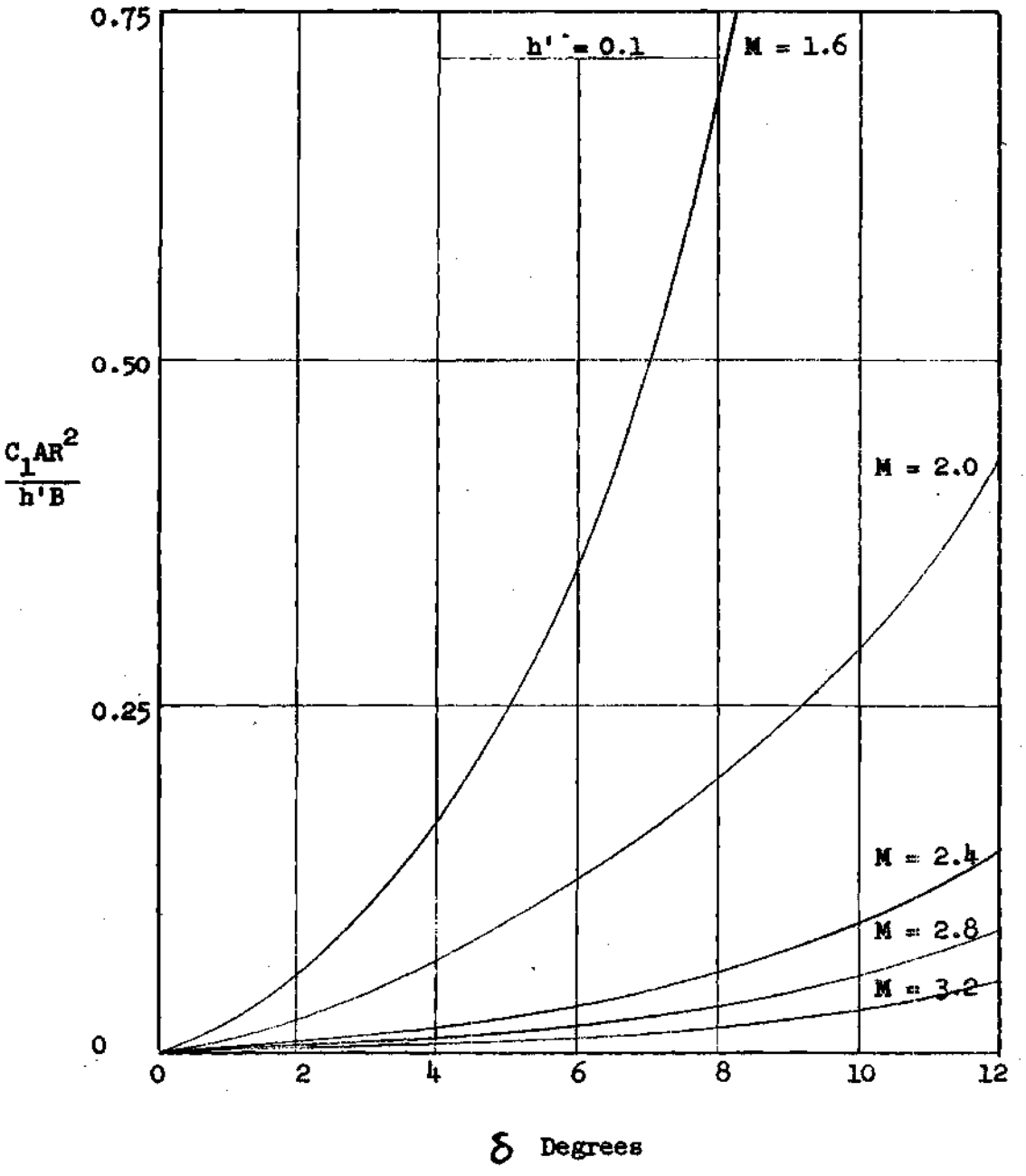

Fig. 14 Rolling Moment Coefficient for a Delta Wing as a Function of Flap Extension Angle for Various Mach Numbers

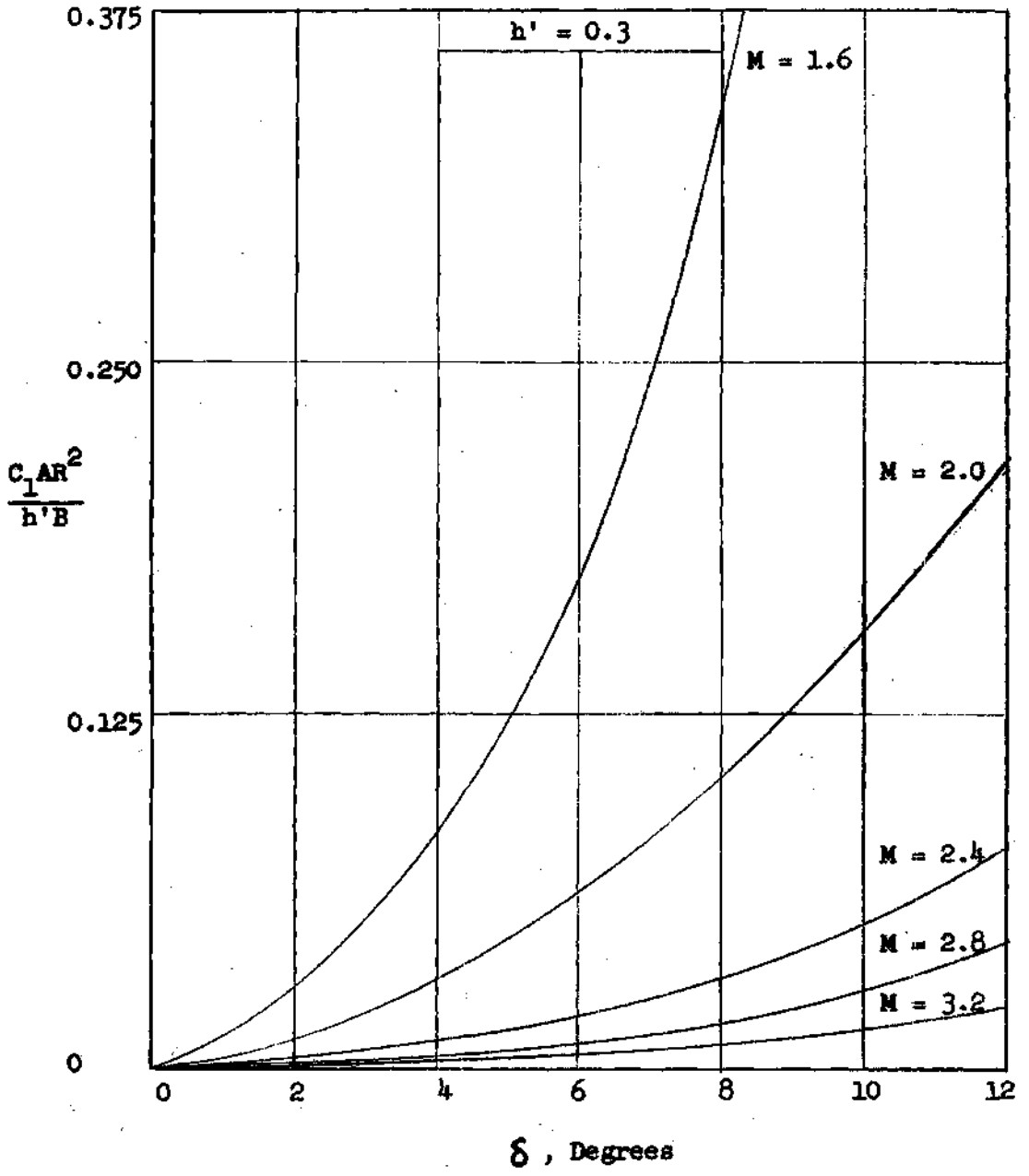

Fig. 14 (Concluded)

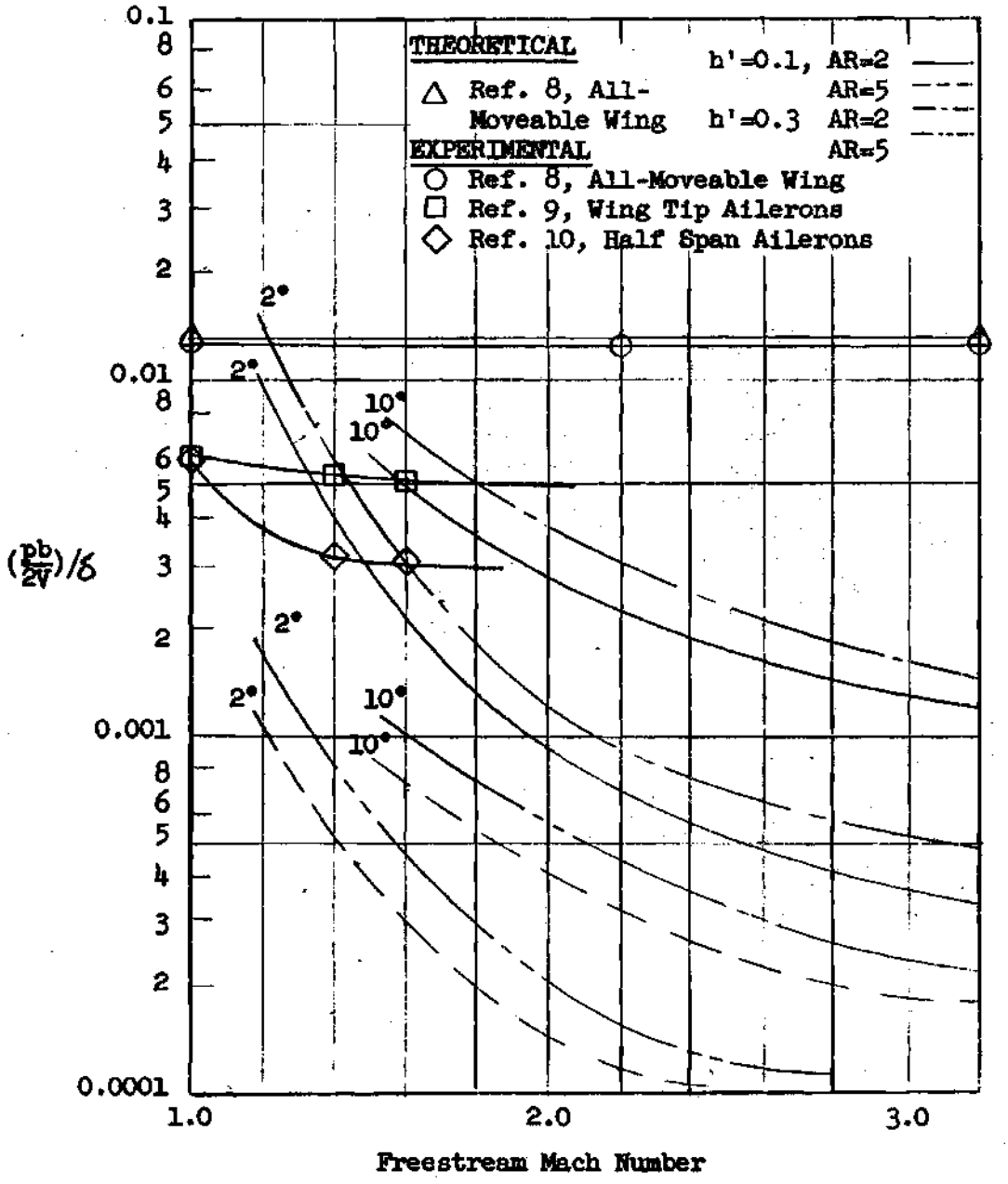

Fig. 15 Rolling Effectiveness for a Rectangular Wing as a Function of Mach Number for Various Aspect Ratios, Flap Heights, and Flap Extension Angles

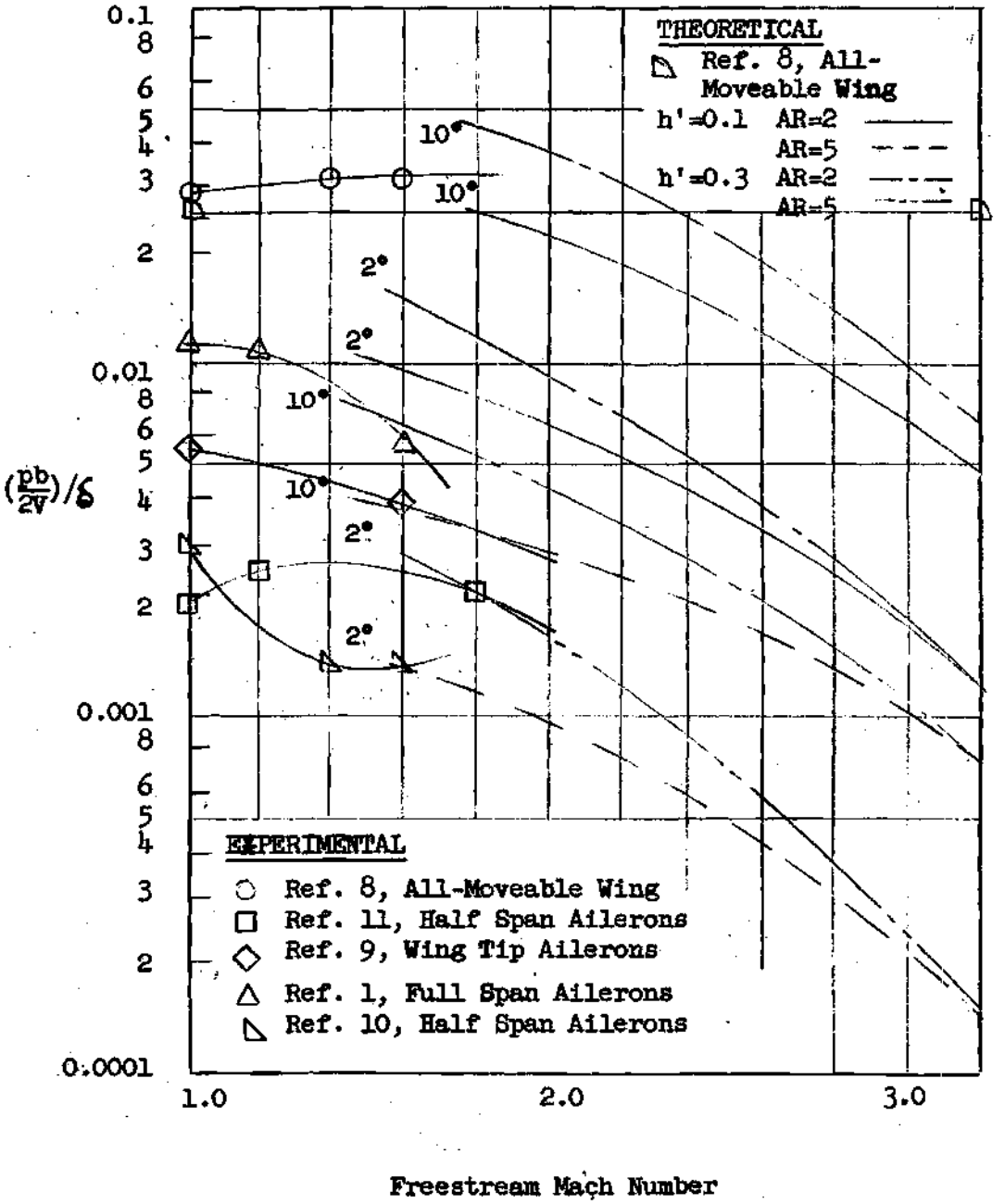

Fig. 16 Rolling Effectiveness for a Forty-Five Degree Swept Wing as a Function of Mach Number for Various Aspect Ratios, Flap Heights, and Flap Extension Angles

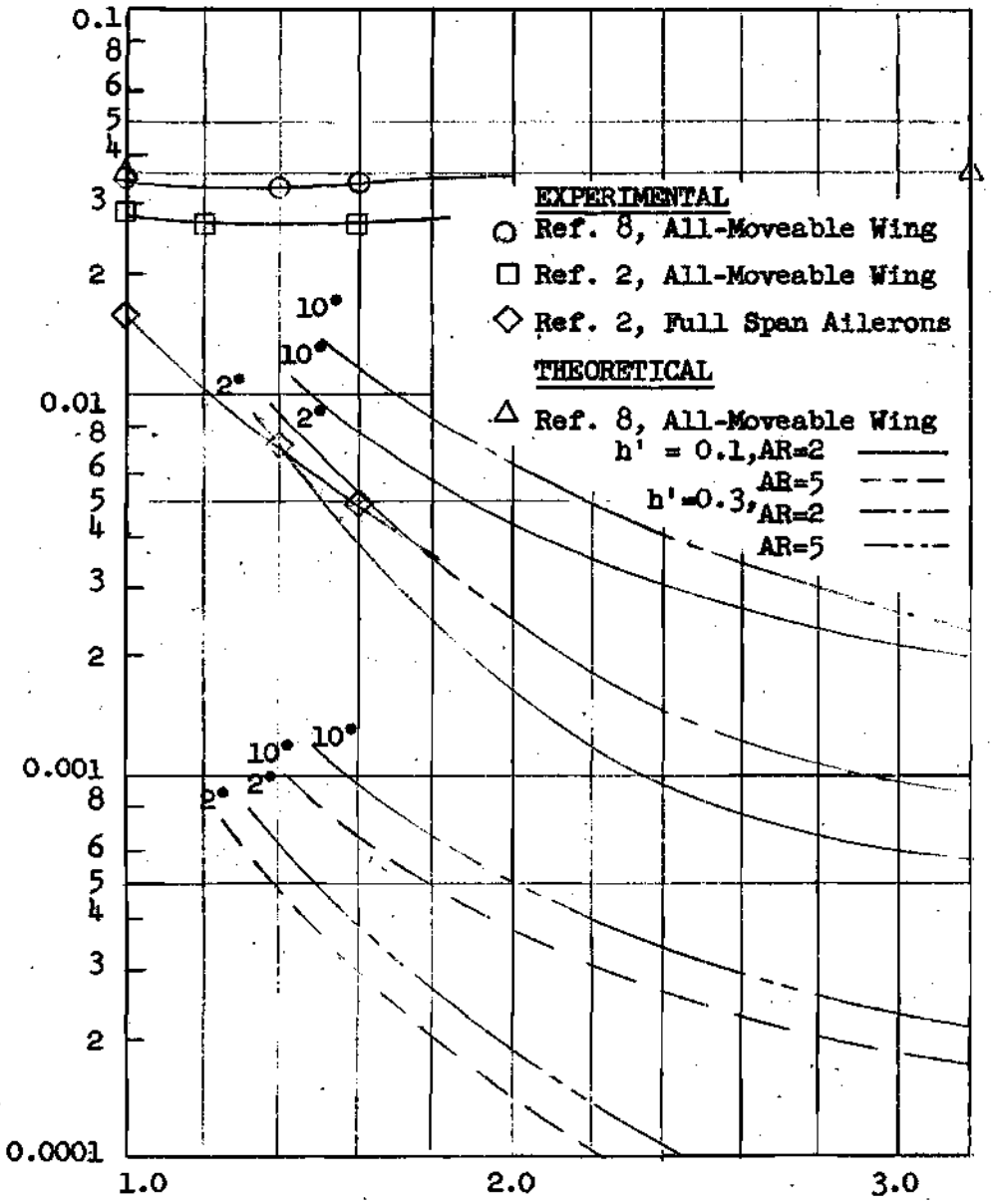

Fig. 17 Rolling Effectiveness for a Delta Wing as a Function of Mach Number for Various Aspect Ratios, Flap Heights, and Flap Extension Angles

CHAPTER IV

DRAG

The drag of the fuselage flap was determined by assuming that the flap is a two-dimensional wedge at zero angle of attack and applying shock-expansion theory. The two-dimensional assumption neglects the effect of pressure reduction due to the influence of freestream conditions above the flap behind the Mach cone emanating from the top portion of the flap (see Fig. 18). The assumption of two-dimensional flow yields a conservative result since the three-dimensional effect reduces the pressure which creates drag force.

Also neglected in the drag determination were the effects of shock impingement on the wing boundary layer and viscous drag. As mentioned in Chapter II, viscous effects were neglected to limit the scope of this presentation.

The drag was found by adding the sum of the pressure forces, determined from shock-expansion theory, in the axial direction. The pressure on the forward portion of the flap, which is constant assuming two-dimensional flow, was found from oblique shock relations for a perfect gas. The pressure on the rear portion of the flap, which is also constant, was found by assuming an isentropic expansion around the flap vertex and using the Prandtl-Meyer expressions[12] for determining the ambient pressure. The resultant pressure multiplied by the cross-sectional area normal to the axial direction gave the drag force.

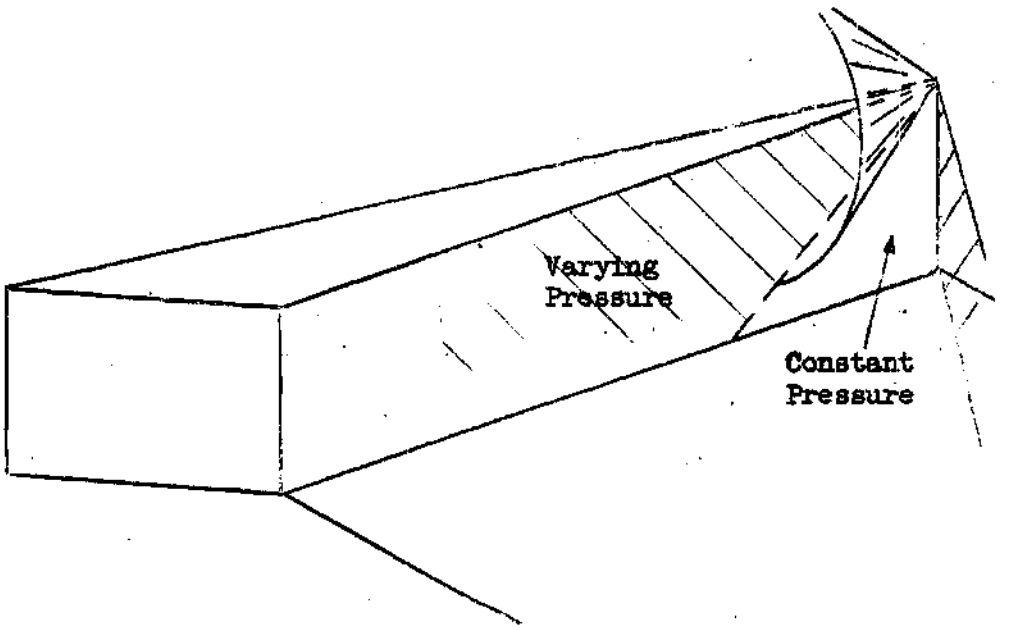

Fig. 18 Mach Cone from the Leading Edge of the Fuselage Flap Showing the Area of Varying Pressure

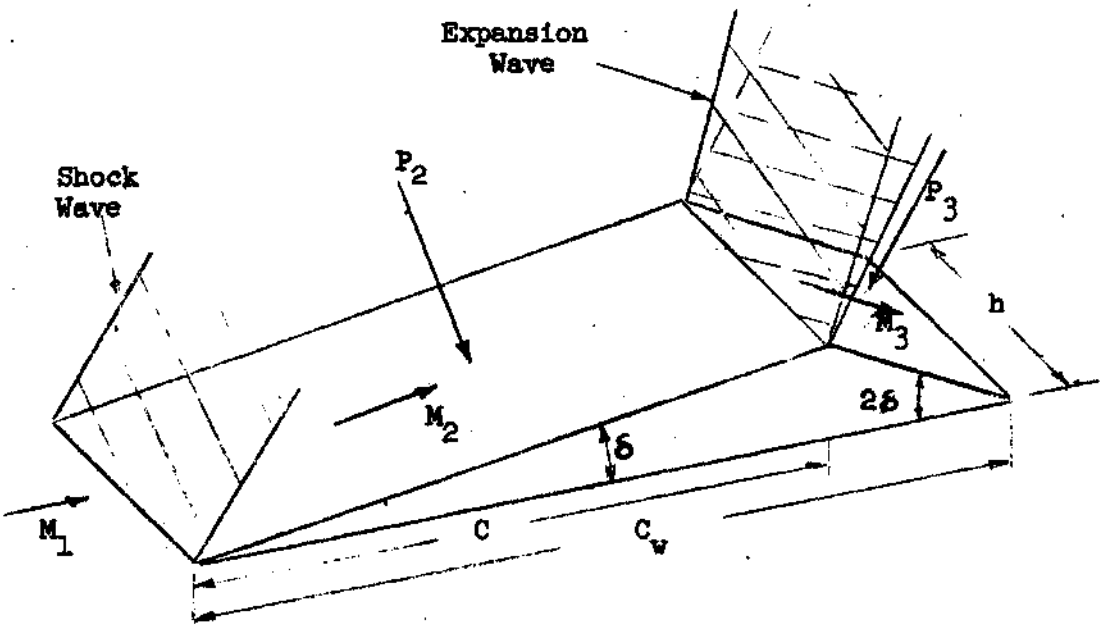

Fig. 19 Pressure Forces Acting on the Control Flap

Noting Fig. 19, the drag can be written as

$$D = hc \tan \delta (P_2 - P_3) \tag{4.1}$$

or, in terms of the drag coefficient based on exposed wing plan form area for a wing with no taper, as

$$C_D = \frac{2h' \tan \delta}{M_1^2 AR} \frac{P_2}{P_1} \left(1 - \frac{P_3}{P_2}\right) \tag{4.2}$$

A correlated plot of drag coefficient versus Mach number, Fig. 20, has been constructed for design purposes. For comparative purposes the drag coefficient has been plotted versus Mach number in Figs. 21 for aspect ratios of two, three, four, and five and flap heights of 0.1c and 0.3c. Experimental drag coefficients found in literature[2,9,14,16,17] for various control system configurations have been compared to the control system discussed in this paper, according to the wing aspect ratio in which they apply. Also included in Figs. 21 is a theoretical drag coefficient for a half-span aileron with chord 0.35c and a deflection angle of six degrees found by shock-expansion theory neglecting three-dimensional effects.

The results of the comparison show that the fuselage flap has a lower drag than aileron configurations for flap extensions of six degrees or less. The theoretical drag coefficient for the half-span ailerons was of the same order of magnitude as the theoretical drag coefficient for the fuselage flap of height 0.1c at extension angles of approximately nine, eleven, twelve, and thirteen degrees at aspect ratios of two, three,

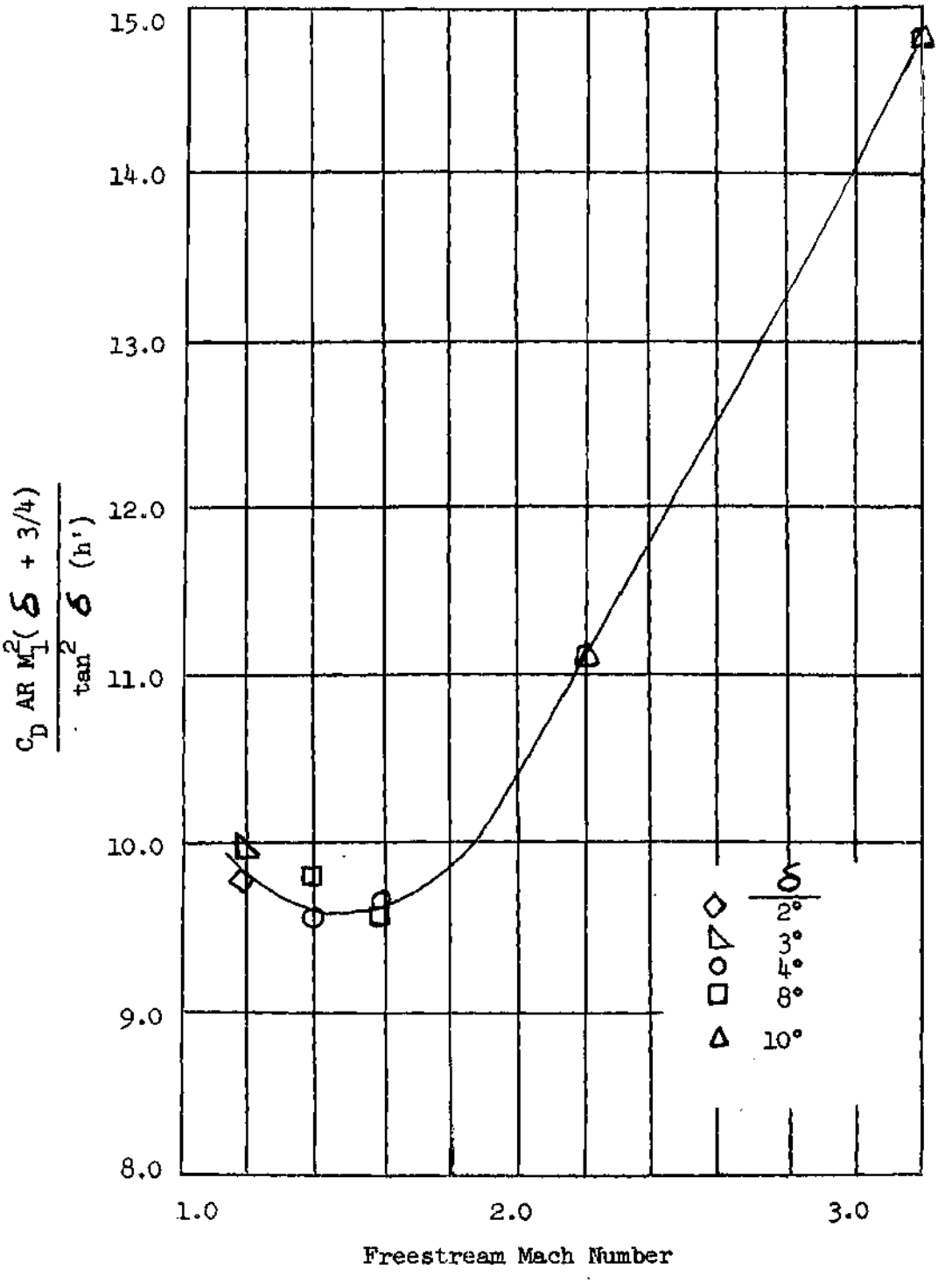

Fig. 20 Fuselage Flap Drag Coefficient as a Function of Mach Number for Various Aspect Ratios, Flap Heights, and Flap Extension Angles

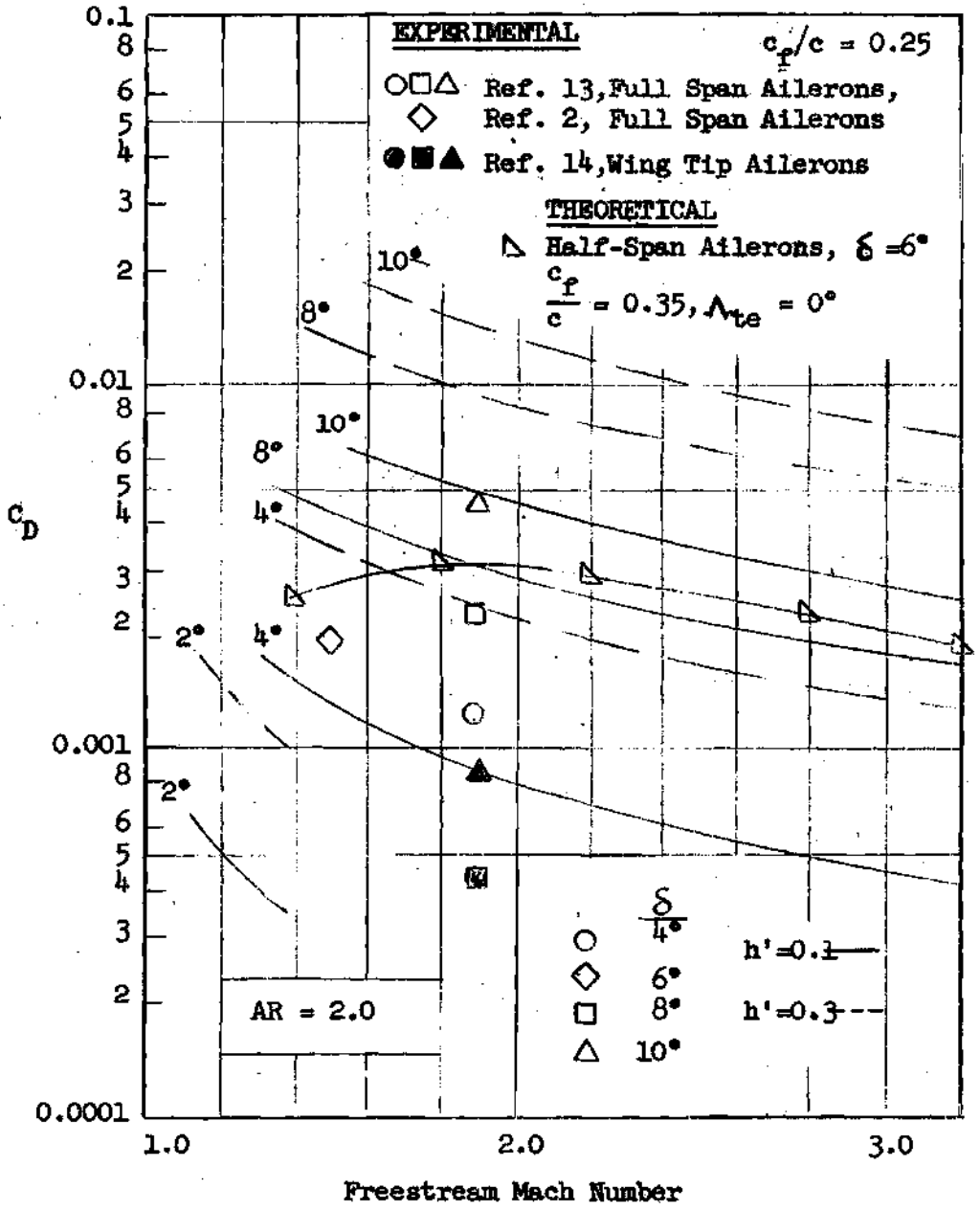

Fig. 21 Fuselage Flap Drag Coefficient as a Function of Mach Number for Various Flap Heights and Flap Extension Angles

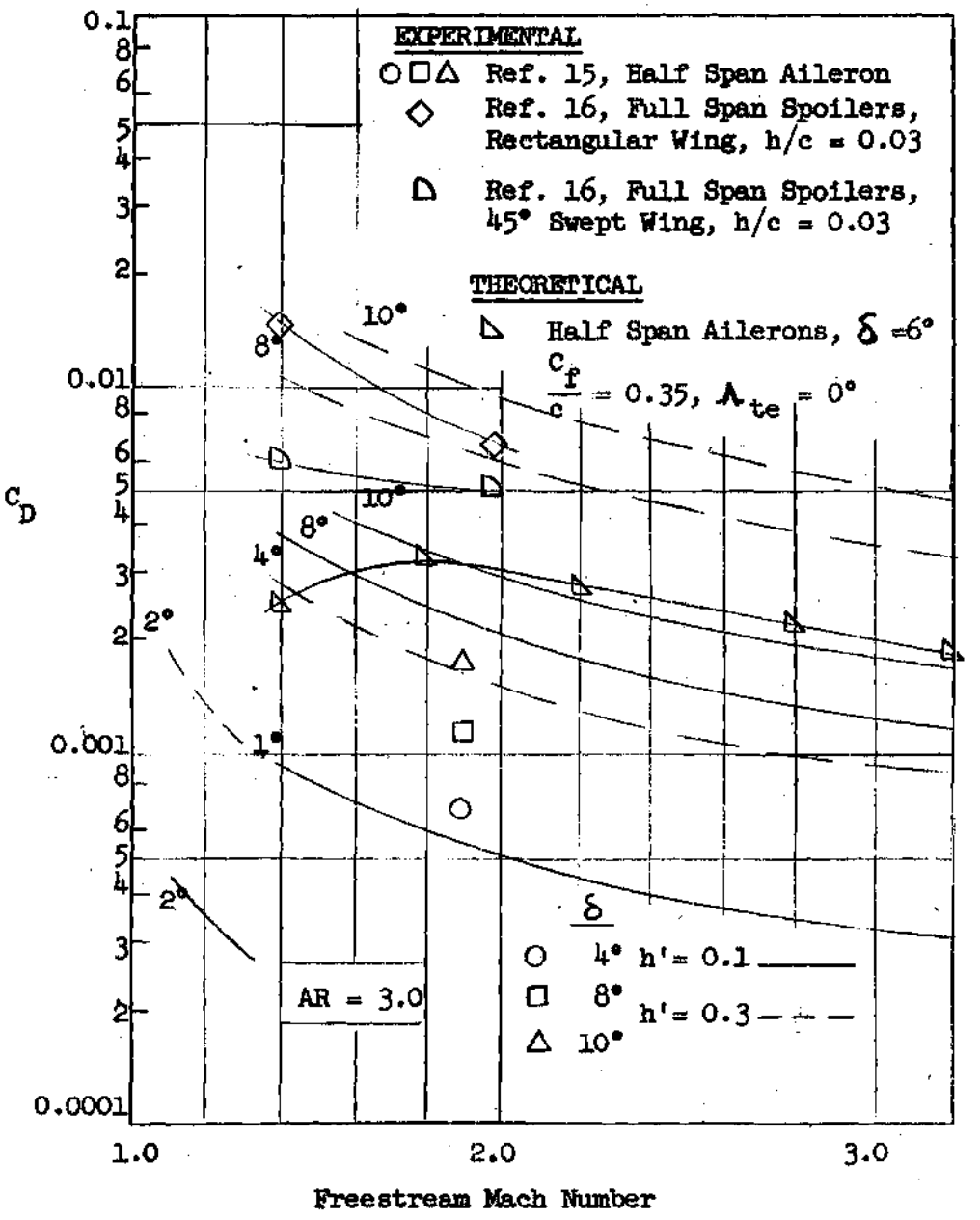

Fig. 21 (Continued)

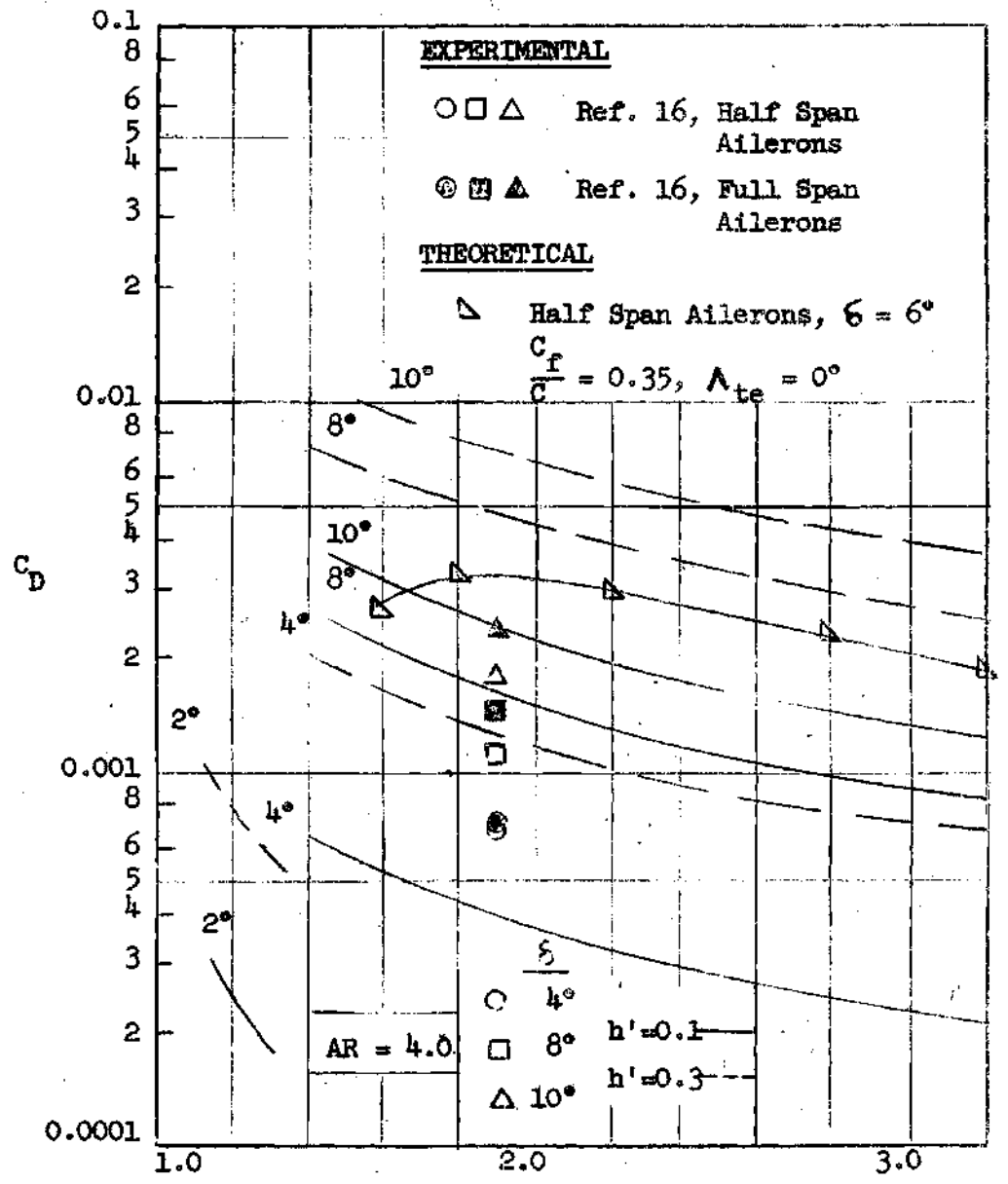

Fig. 21 (Continued)

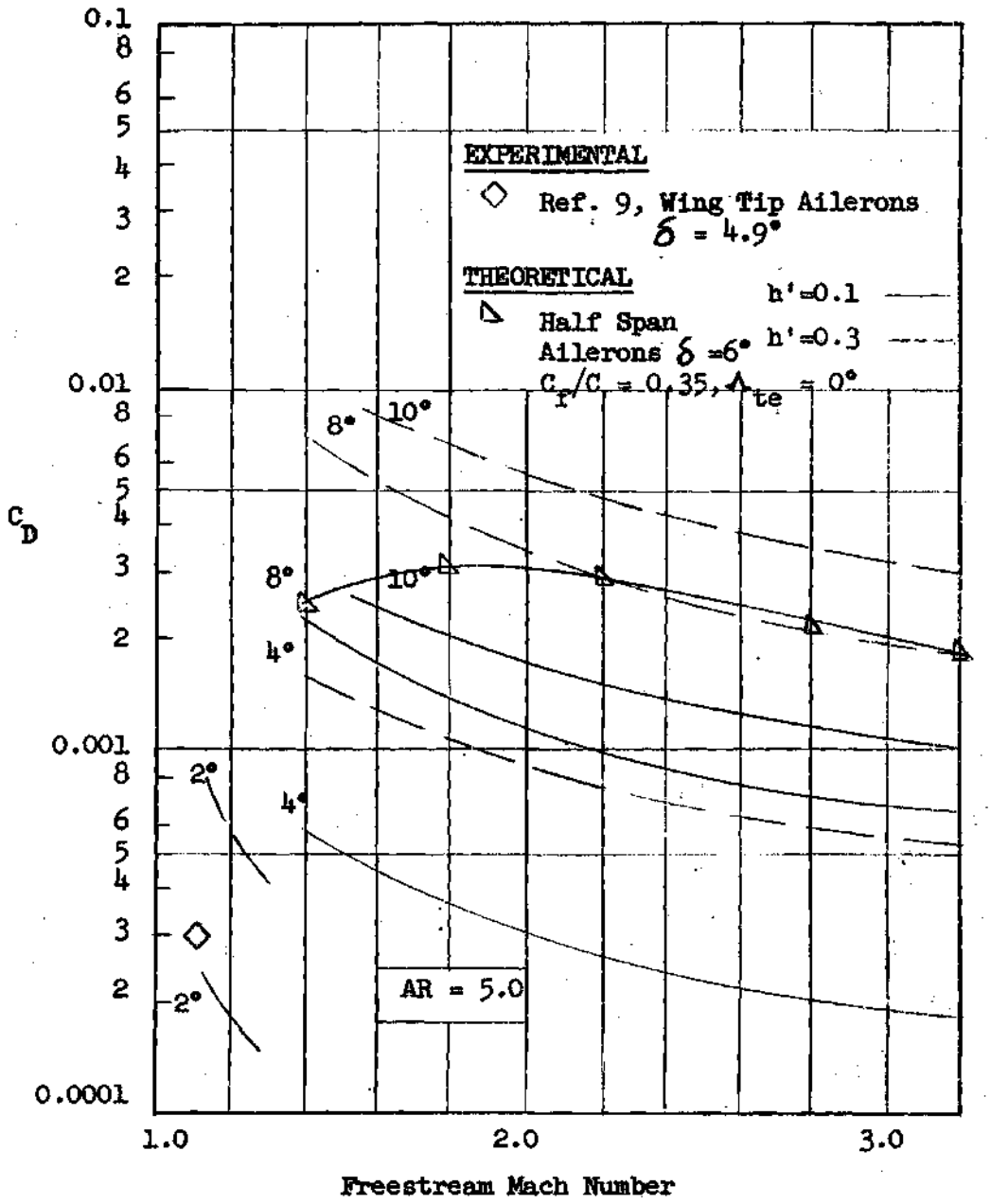

Fig. 21 (Concluded)

four, and five, respectively. The theoretical drag coefficient for the aileron over-estimated the experimental values because three-dimensional effects were neglected, however, three-dimensional effects were also neglected in determining the fuselage flap drag coefficient; therefore, a better estimate is obtained for the drag coefficient between the fuselage flap and the half-span ailerons when theoretical results are used. Results of the drag comparison between full span spoilers and the fuselage flap (see Fig. 21, AR = 3.0) showed that for flap heights of 0.1c, the spoiler does not compare favorably; however, for a flap height of 0.3c comparable drag coefficients were obtained. The experimental drag coefficient for wing tip ailerons was substantially lower than the drag coefficient for the fuselage flap for the aspect ratios and Mach numbers at which experimental data was obtained.

To restrict the length of this investigation a comparison was not made of the rolling moment coefficient as a function of the drag coefficient for the control systems under consideration.

CHAPTER V

CONCLUSIONS

The results of this investigation of the fuselage flap control system have indicated that:

1. The fuselage flap control system used in conjunction with a rectangular wing affords adequate roll control between the Mach numbers of 1.2 and 1.8.

2. The fuselage flap used with a forty-five degree swept wing is an excellent control device for Mach numbers between 1.4 and 2.2.

3. For a delta wing plan form, the fuselage flap affords adequate roll control for Mach numbers between 1.2 and 2.2.

4. For the range of Mach numbers investigated, the fuselage flap compares favorably with all types of conventional control systems other than the all-moveable wing system.

5. The fuselage flap control system of height 0.1c has a comparable or smaller drag coefficient compared to that of conventional control systems other than wing tip ailerons.

6. The drag coefficients obtained for the fuselage flap of height 0.3c are larger than those for conventional controls with the exception of spoilers. In this case comparable drag coefficients were obtained.

7. Overall results indicate that the fuselage flap control system is comparable to conventional control systems, excepting all-moveable wings.

8. The rolling effectiveness, $(\frac{pb}{2V})/\delta$, is not a satisfactory com-

parison parameters since the term C_{l_δ} used in its determination is not linear. This implies that the rolling effectiveness, which is usually not a function of the deflection angle, is a function of the fuselage flap extension angle.

CHAPTER VI

RECOMMENDATIONS

It is recommended that any further study of the fuselage flap control system include the effects of viscosity. This could be done by investigating the effects on drag of the shock wave impinging on the wing boundary layer. Research for literature covering the normal shock wave impingement on a boundary layer at a Mach number greater than 1.0 revealed that few or no studies have been made in this field. Also, further investigation should include viscous drag.

Wind tunnel tests of the fuselage flap control system should be performed to substantiate the data obtained in this investigation. The loads on the wing from these tests should be used to determine the effect of aeroelasticity on the rolling moment.

There should be a study made on the control forces required to activate the control flap and a comparison made with control forces required to activate conventional control systems.

Consideration should be given to the fuselage flap as a pitching and yawing control device.

It is also recommended that a more satisfactory rolling effectiveness parameter be devised to take into account the non-linearity of the fuselage flap rolling moment coefficient.

APPENDIX I

VERIFICATION OF THE NON-INTERACTION OF THE FUSELAGE FLAP SHOCK WAVE AND EXPANSION WAVE ON THE WING SURFACE

Since no explicit relation exists between the flap extension angle, δ, and the shock angle, θ, a geometrical approach was used here to show that the expansion wave from the rear of the fuselage flap does not intersect the shock wave within the wing boundary. The intersection would cause a curved shock and a varying pressure coefficient along the shock.

From Fig. 22, the plot of shock angle versus flap extension angle, the shock angles were found for various Mach numbers and constant flap extension angles. With the shock angles known the Mach number downstream of the shock was found from perfect gas relations which led to the determination of the Mach angle. This procedure was carried out for flap extensions of two and ten degrees and the angles were plotted on a wing plan form which varied in aspect ratio (see Figs. 23 and 24).

It can be seen that the shock and expansion waves do not intersect within the wing boundaries for the aspect ratios under consideration.

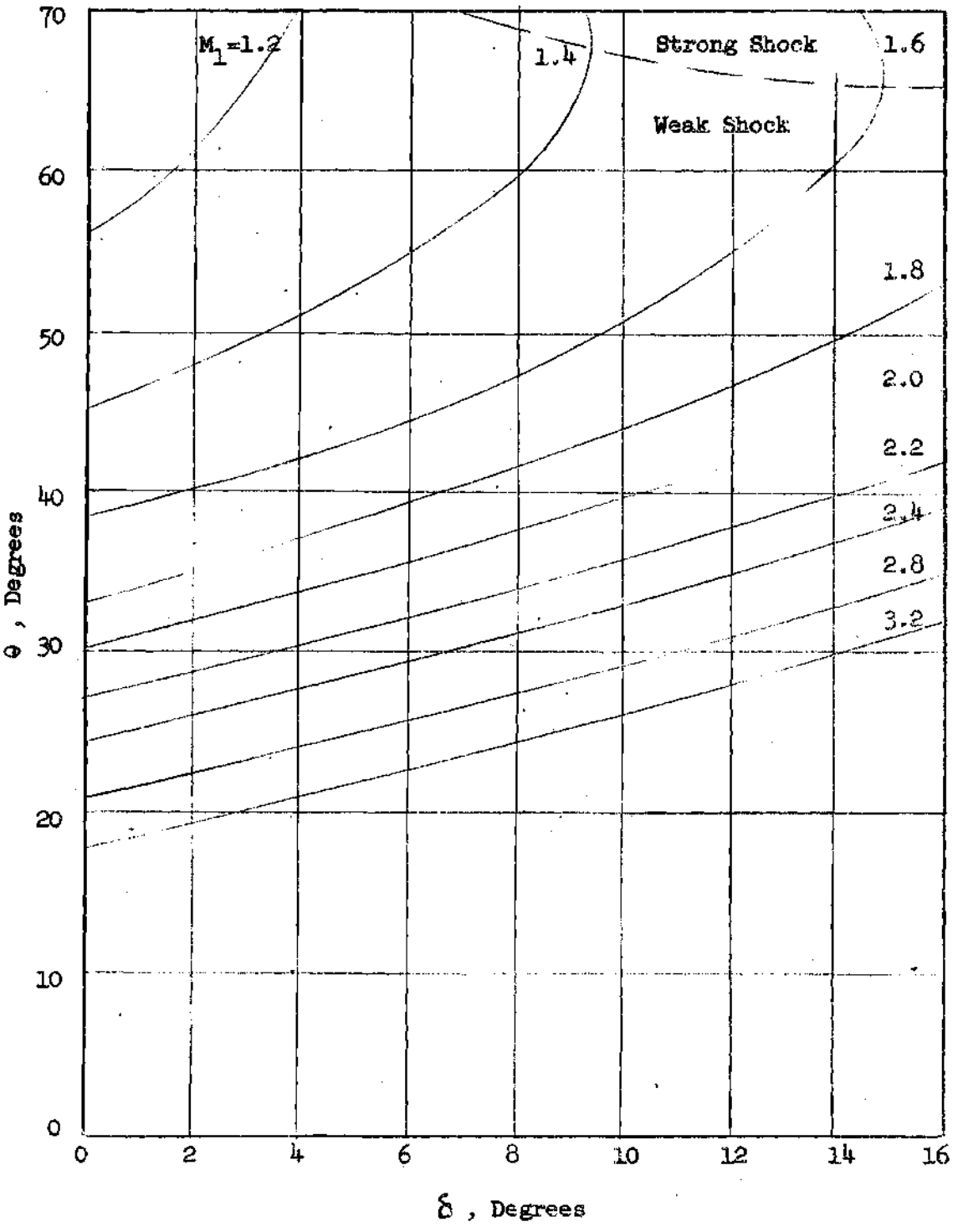

Fig. 22 Variation of Shock Wave Angle with Flap Extension Angle for Various Upstream Mach Numbers

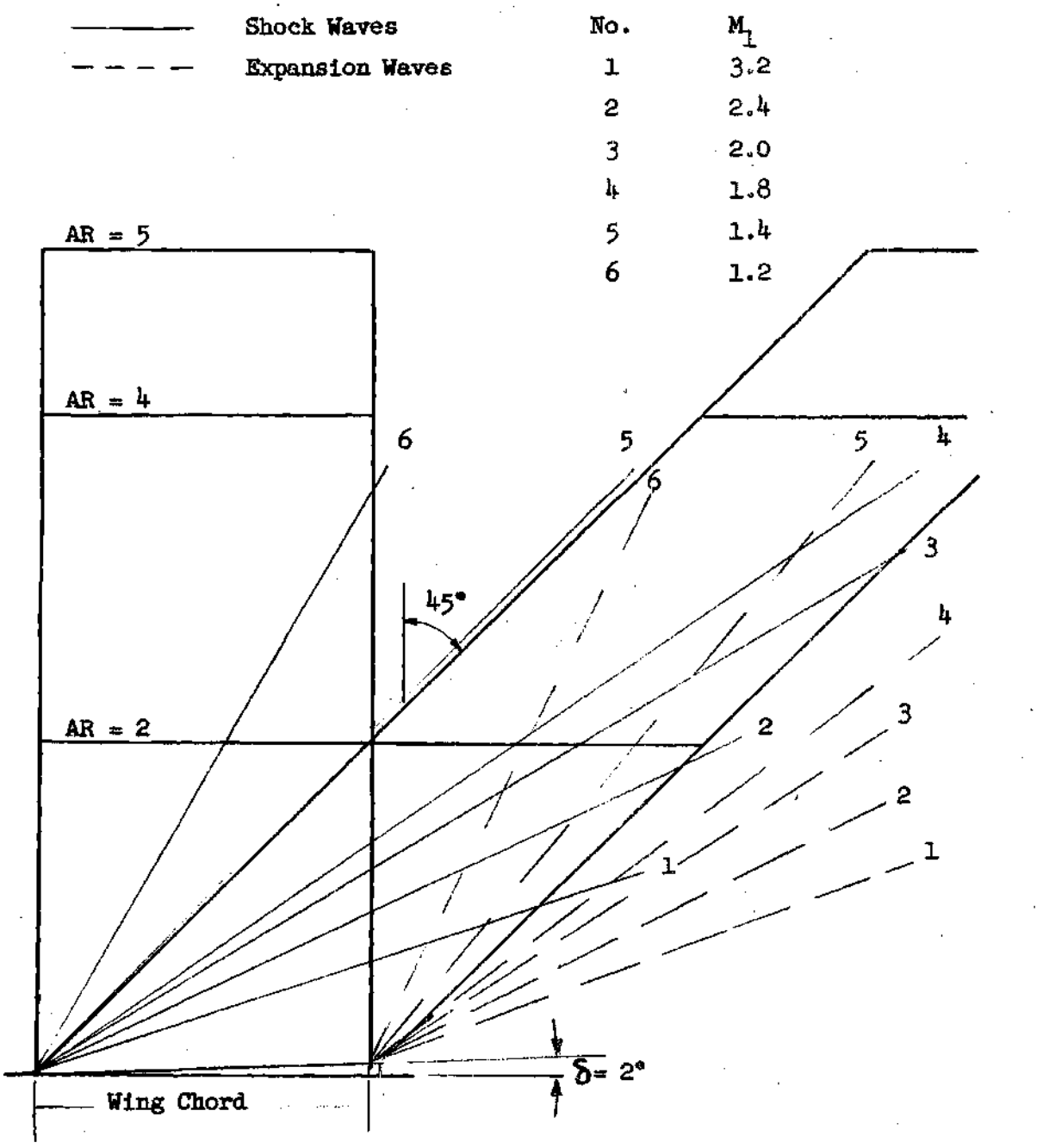

Fig. 23 Shock Wave and Expansion Wave Angles for Various Mach Numbers and a Flap Extension Angle of Two Degrees

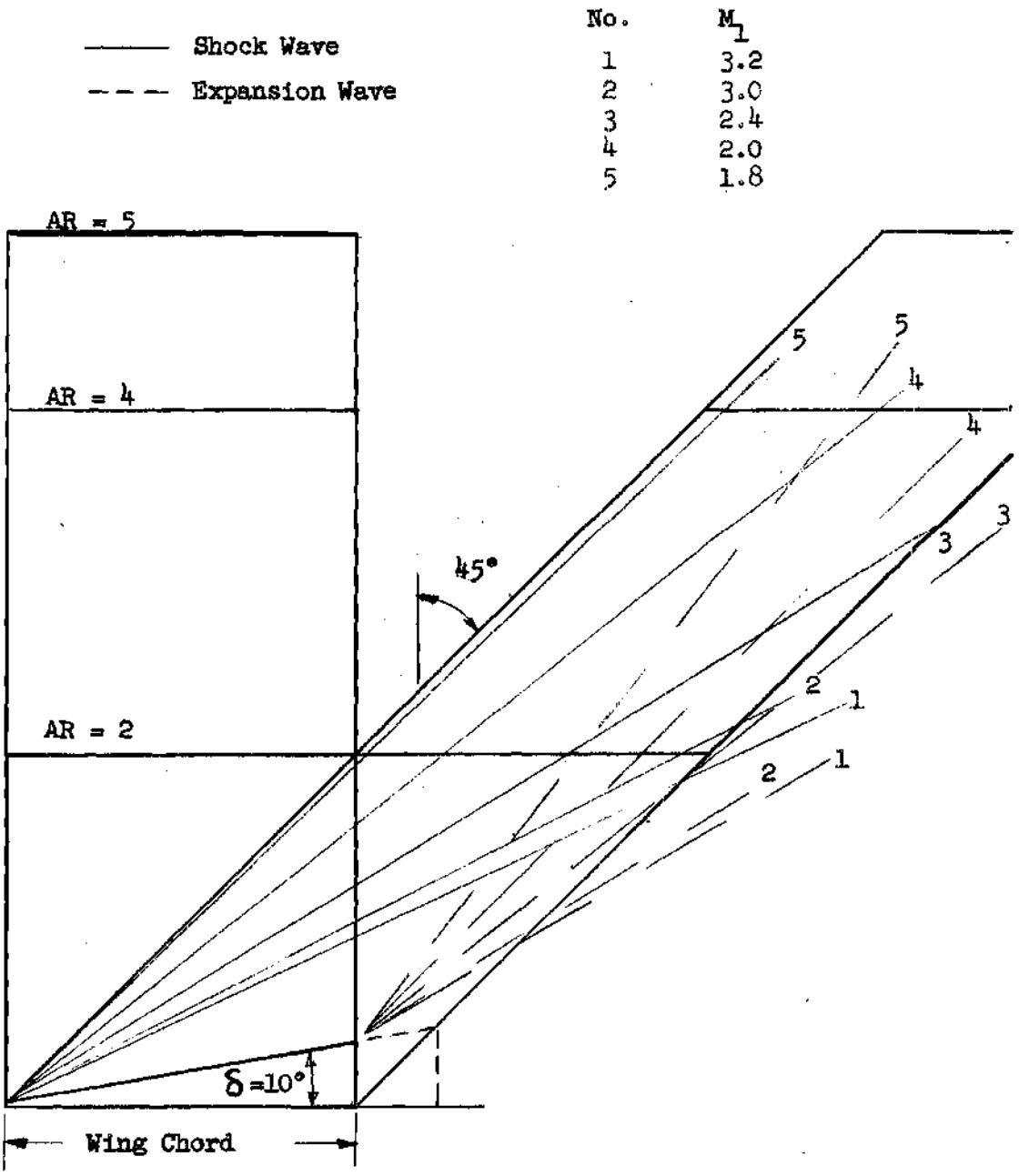

Fig. 24 Shock Wave and Expansion Wave Angles for Various Mach Numbers and a Flap Extension Angle of Ten Degrees

APPENDIX II

DETERMINATION OF THE THREE-DIMENSIONAL LIFT-CURVE SLOPE

In the wing tip region the lift is given by

$$C_L = \int_0^{\mu_1} C_p \cdot \frac{dA}{S} \tag{A.1}$$

where, from Busemann[17] and Nielson[18],

$$C_p = \frac{4}{B_o} \frac{\cos^{-1}}{\pi} (1 - 2 B_o \tan \alpha) \tag{A.2}$$

and from Fig. 25 with the wing tip chord parallel to the flight direction

$$dA = \frac{c^2 \, d\alpha}{2(\sin \alpha \tan \Lambda_{te} + \cos \alpha)^2}$$

For a taper ratio of one the lift is then given by

$$C_L = \frac{2\alpha_o}{B_o \pi AR} \int_0^{\mu_1} \frac{\cos^{-1}(1 - 2 B_o \tan \alpha)}{(\sin \alpha \tan \Lambda + \cos \alpha)^2} \, d\alpha \tag{A.3}$$

where α_o is the angle of attack of the wing. The lift-curve slope is then given by

$$a_o = \frac{dC_l}{d\alpha_o} = \frac{2}{B_o \pi AR} \int_0^{\mu_1} \frac{\cos^{-1}(1 - 2B_o \tan \alpha) \, d\alpha}{(\sin \alpha \tan \Lambda + \cos \alpha)^2} \tag{A.4}$$

Equation (A.4) was integrated by parts to give the lift-curve slope in the wing tip region for a forty-five degree swept wing:

$$a_o = \frac{1}{B_o \cdot AR}\left[\frac{2B_o - 1}{\sqrt{(2B_o + 1)^2 - 1}} - \frac{B_o - 1}{B_o + 1}\right] \tag{A.5}$$

The loss in lift curve slope due to three-dimensional effects was determined by subtracting the Equation (A.5) from the two-dimensional lift curve slope given by Ackeret theory, $\frac{4}{B_o}$. Thus,

$$a_{o_{Loss}} = \frac{1}{AR}\left[1 - \frac{2B_o - 1}{\sqrt{(2B_o + 1)^2 - 1}}\right] \tag{A.6}$$

The total lift curve slope for the wing is

$$a_o = \frac{4}{B_o} - a_{o_{Loss}} \tag{A.7}$$

Equation (A.7) was substituted into Equation (A.6) to yield

$$a_o = \frac{4}{B_o}\left[1 - \frac{1}{4AR}\left(1 - \frac{2B_o - 1}{\sqrt{(2B_o + 1)^2 - 1}}\right)\right] \tag{A.8}$$

Similarly, the lift-curve slope for a rectangular wing is

$$a_o = \frac{4}{B_o}\left(1 - \frac{1}{2B_o AR}\right) \tag{A.9}$$

For a delta wing there is no loss at the wing tip, therefore the lift curve-slope is the same as that for two-dimensional flow. Or,

$$a_o = \frac{4}{B_o} \qquad \text{(A.10)}$$

APPENDIX III

DERIVATION OF THE ROLLING MOMENT COEFFICIENT EQUATIONS

As explained in Chapter III, the total rolling moment coefficient will be found by subtracting the losses in rolling moment coefficient due to three-dimensional effects from the coefficient which would be obtained if a constant pressure existed on the wing behind the shock wave.

Loss in Rolling Moment Coefficient due to a Pressure Influence above the Shock Wave.--For this particular case the pressure coefficient was integrated between the Mach angle and the angle at which a line from the top of the shock wave no longer intersected the wing surface (see Fig. 26). This expression was then integrated spanwise to give the final rolling moment coefficient in region I. Note that the cone angle from the top of the shock front was assumed to be equal to Mach angle based on the Mach number behind the shock (see p. 8).

The rolling moment coefficient is given by

$$C_l = C_p \cdot \frac{2y}{b} \cdot \frac{dA}{S} \tag{A.11}$$

where

$$C_p = C_{p_s} \cdot \frac{\cos^{-1}}{\pi} (1 - 2 B \tan \alpha) \tag{A.12}$$

Since the rolling moment was to be determined using oblique shock wave theory the shock wave pressure coefficient, C_{p_s}, was substituted

for the linearized pressure coefficient, $\frac{4\alpha}{B_o}$, in Equation (A.2).

The incremental area dA was found geometrically from Fig. 26 to be

$$dA = \frac{h \cdot d\alpha \cdot dy}{\sin^2 \alpha} \tag{A.13}$$

Substitution of Equations (A.12) and (A.13) into Equation (A.11) yields for a wing with a taper of one

$$C_l = \frac{C_{p_s} \cdot h'}{2\pi} \int_o^{y^*} \int_{\alpha_m}^{\mu} \frac{\cos^{-1}(1 - 2B \tan \alpha)}{\sin^2 \alpha} \cdot y' \cdot dy' \cdot d\alpha \tag{A.14}$$

where α_m is the angle at which the ray from the point of disturbance no longer intersects the wing surface, and y^* is the upper limit of the spanwise integration.

The term y^* was determined for the shock angle less than ϕ for arbitrary wing by noting from Fig. 27 that

$$y_e = \frac{(c - hB) \tan \theta}{1 - \tan \Lambda_{te} \tan \theta} \tag{A.15}$$

or

$$y^* = \frac{2y_e}{b} = \frac{2(1 - h'B) \tan \theta}{AR(1 - \tan \Lambda_{te} \tan \theta)} \tag{A.16}$$

For the shock angle greater than ϕ and hB less than the remaining tip chord, c_s, behind the shock wave, the limit of integration is then given by

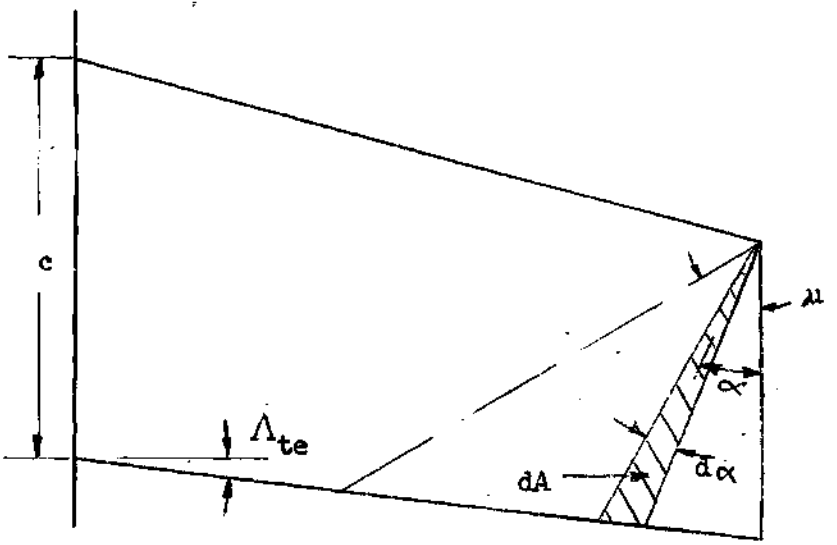

Fig. 25 Planview of Wing Showing the Area of Integration in Determining the Three-Dimensional Lift-Curve Slope

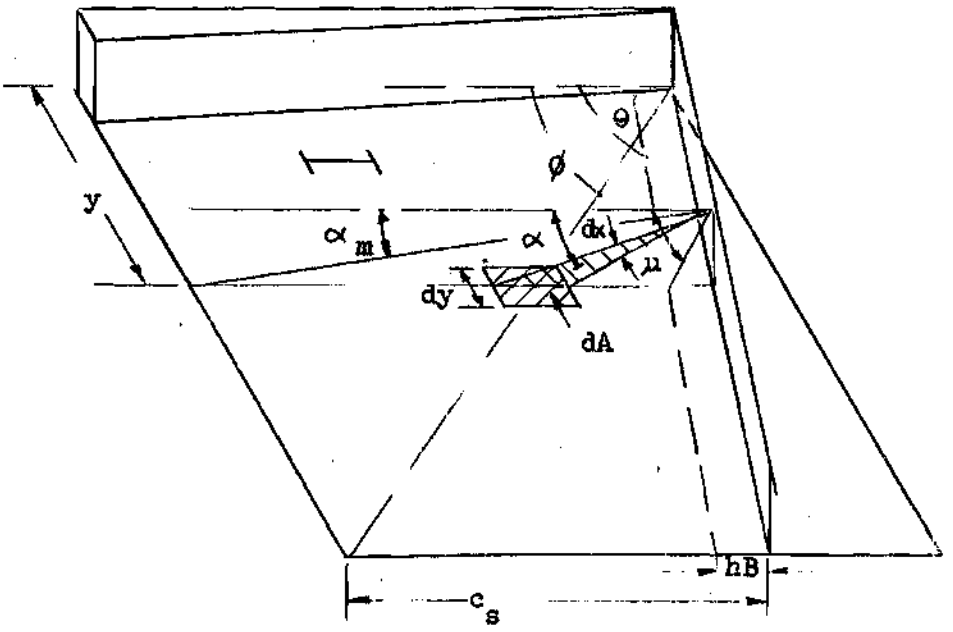

Fig. 26 Incremental Area used in the Determination of the Rolling Moment Coefficient in Region I

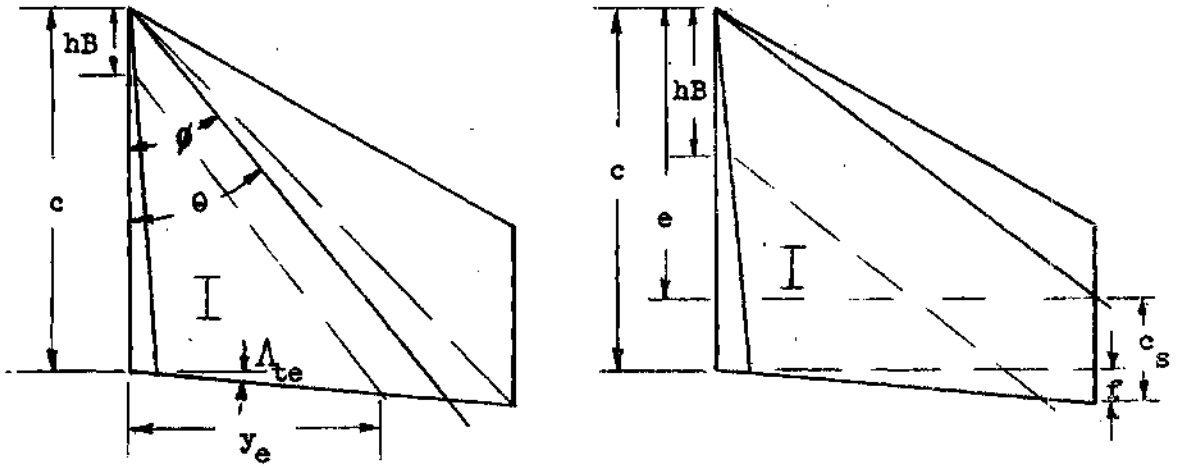

Fig. 27 Configuration for Determining the Upper Limit of Integration in Region I

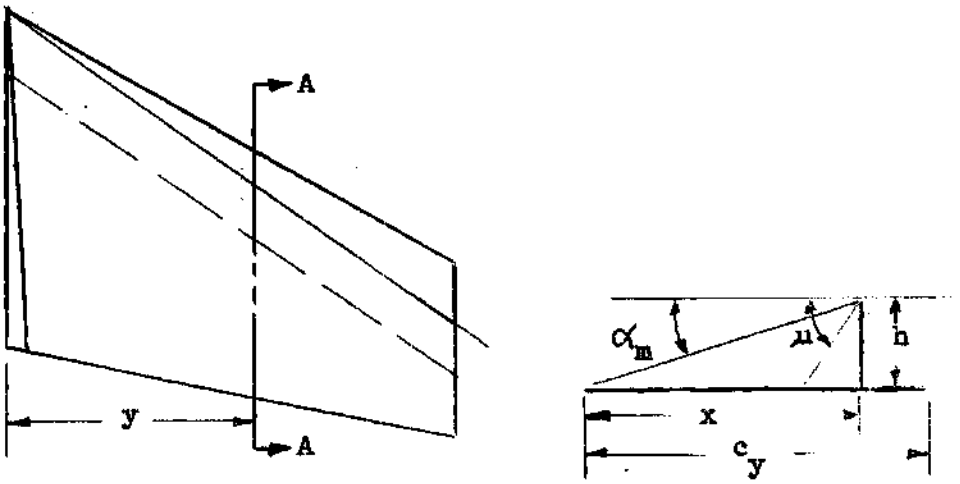

Fig. 28 Configuration for Determining the Lower Limit of Integration in Region I

$$y^* = 1.0 \tag{A.17}$$

When hB is greater than c_s the same situation exists as in the case of the shock angle less than ϕ. Thus,

$$y^* = \frac{2(1 - h'B) \tan \theta}{AR(1 - \tan \Lambda_{te} \tan \theta)} \tag{A.18}$$

Referring to Fig. 27, the term hB is greater than c_s when

$$hB > c - e + f$$

or,

$$hB > c - \frac{b}{2 \tan \theta} - \frac{b \tan \Lambda_{te}}{2} \tag{A.19}$$

In non-dimensional form Equation (A.19) becomes

$$h'B > 1 - \frac{AR}{2} \left[\frac{1 - \tan \Lambda_{te} \tan \theta}{\tan \theta} \right] \tag{A.20}$$

The lower limit of integration of Equation (A.14), α_m, is a function of the distance along the span. Referring to Fig. 28, it can be seen that

$$\alpha_m = \tan^{-1} \left(\frac{h}{x} \right) \tag{A.21}$$

where x is determined from an arbitrary wing plan form, Fig. 28, to be

$$x = c - y \left[\frac{(1 - \tan \Lambda_{te} \tan \theta)}{\tan \theta} \right]$$

Equation (A.21) then becomes, in non-dimensional form,

$$\alpha_m = \tan^{-1}\left[\frac{h'}{1 - \frac{AR.y'}{2}\frac{(1 - \tan \Lambda_{te} \tan \theta)}{\tan \theta}}\right] \qquad (A.22)$$

Equation (A.14) was integrated once with respect to α to get

$$C_l = \frac{C_{p_s} \cdot h'B}{2} \int_o^{y^*} \left[\frac{(1 - ty')}{h'B} \cos^{-1}\left(1 - \frac{2h'B}{1 - ty'}\right) + 2\sqrt{\frac{1 - ty'}{h'B} - 1} - \pi\right] y' \cdot dy' \qquad (A.23)$$

where

$$t = \frac{AR}{2}\frac{(1 - \tan \Lambda_{te} \tan \theta)}{\tan \theta}$$

It was more convenient to find a loss in rolling moment coefficient in each region and subtract this value from the rolling moment that would be obtained if the pressure coefficient on the wing surface behind the shock were constant.

The constant pressure rolling moment coefficient is given by the product of the area, the moment arm, and the shock wave pressure coefficient, as determined geometrically from Fig. 29. For the shock angle greater than ϕ and hB less than c_s the affected area in non-dimensional form in region I is given by

$$A' = \frac{A}{S} = \frac{2(1 - h'B) - t}{4} \qquad (A.24)$$

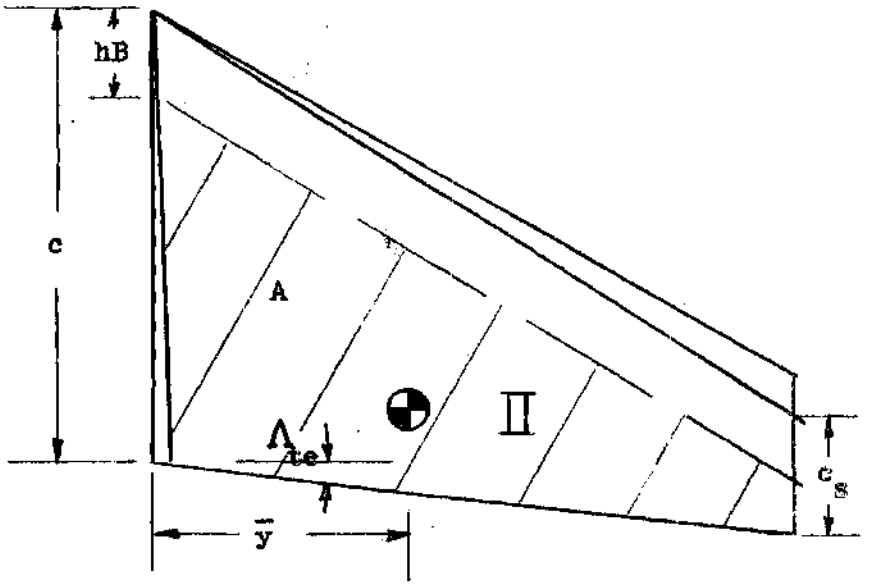

Fig. 29 Configuration for Determining the Constant Pressure Rolling Moment Coefficient in Region I

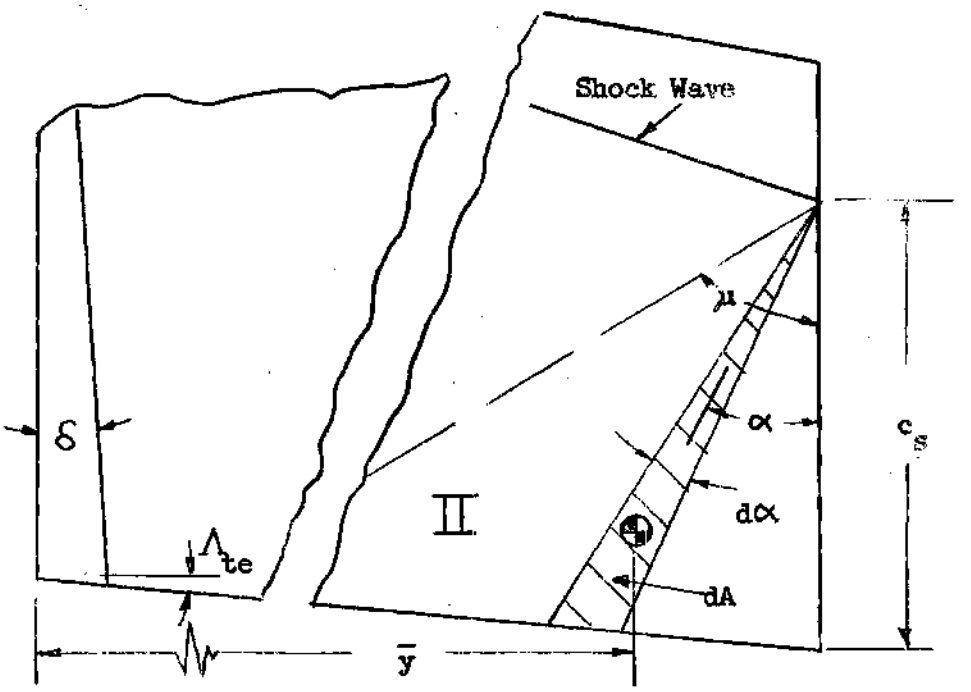

Fig. 30 Configuration for Determining the Loss in Rolling Moment Coefficient due to Tip Effect Behind the Shock Wave

and the moment arm from the root chord is

$$\bar{y}' = \frac{2\bar{y}}{b} = \frac{\frac{1}{2}(1 - h'B) - \frac{t}{3}}{(1 - h'B) - \frac{t}{2}} \tag{A.25}$$

When Θ is greater than ϕ and hB is greater than c_s, the affected area in region I is

$$A' = \frac{(1 - h'B)^2}{2 \cdot AR \cdot t} \tag{A.26}$$

and the moment arm is

$$\bar{y}' = \frac{2(1 - h'B)}{3 \cdot AR \cdot t} \tag{A.27}$$

For the shock angle less than ϕ the same equations are obtained as Equations (A.26) and (A.27).

For a constant pressure coefficient in region I the rolling moment coefficient is

$$C_{l_s} = C_{p_s} \cdot A' \cdot \bar{y}' \tag{A.28}$$

where A' and $\bar{y}'$ are dependent upon the shock angle and flap height.

The loss in rolling moment coefficient in region I is then given by

$$C_{l_{L_I}} = C_{l_{s_I}} - C_{l_I} \tag{A.29}$$

Tip Effect as a Result of the Shock Wave in Reducing the Rolling Moment Coefficient.--The loss in rolling moment, region II, is a result of the

freestream conditions outside of the wing tip influencing conditions on the wing surface behind the Mach cone from the point of intersection of the shock wave and the wing tip.

Since conical flow has been assumed the pressure coefficient on the incremental area dA is constant. By geometric and trigonometric substitution dA was found from Fig. 30 to be

$$dA = \left(c - \frac{b \cdot T}{2} \right)^2 \frac{d\alpha}{2S^2} \qquad (A.30)$$

where

$$S = \sin \alpha \tan \Lambda_{te} + \cos \alpha$$

and

$$T = \frac{1 - \tan \Lambda_{te} \tan \theta}{\tan \theta}$$

Similarly, the moment arm to the centroid of the incremental area is

$$\bar{y} = \frac{b}{2} - \frac{2\left(c - \frac{b \cdot T}{2}\right)}{3S} \sin \alpha \qquad (A.31)$$

Substitution of Equations (A.30) and (A.31) into Equation (A.11) yields, upon re-arranging,

$$C_{l_{II}} = C_{p_s} \frac{\left(1 - \frac{AR \cdot T}{2}\right)^2}{2 \pi AR} \int_0^{\mu} \frac{\cos^{-1}(1 - 2B \tan \alpha)}{S^2} \left[1 - \right.$$

$$\left. \cdot \; 4 \frac{\left(1 - \frac{AR \cdot T}{2}\right)}{3\,AR} \sin\alpha \right] d\alpha \qquad (A.32)$$

To determine the loss in rolling moment coefficient due to the tip effect it was necessary to find the rolling moment coefficient which would have occured if there were no tip effects, or if the pressure coefficient in region II were constant and the same value as that behind the shock.

By a similar procedure as in region I, the constant pressure rolling moment coefficient in region II was found to be

$$C_{l_{s_{II}}} = \frac{C_{p_s} \cdot \left(1 - \frac{AR \cdot T}{2}\right)^2}{2\,AR\,(\tan \Lambda_{te} + B)} \left[1 - \frac{2\left(1 - \frac{AR \cdot T}{2}\right)}{3\,AR\,(\tan \Lambda_{te} + B)} \right] \qquad (A.33)$$

so that the loss in rolling moment coefficient due to the tip effect in region II became

$$C_{l_{L_{II}}} = C_{l_{s_{II}}} - C_{l_{II}} \qquad (A.34)$$

Tip Effect as a Result of Mach Waves in Reducing the Rolling Moment Coefficient.--The final region in which a loss in rolling moment occurs is that which is created by the intersection of the Mach wave from the top of the shock wave and the wing tip (see Fig. 11).

In region III conical flow theory is no longer valid and the equations for determining the variation in pressure coefficient lose their linearity; however, for the purpose of this presentation a conical flow field is assumed. In the equation for the variation of pressure coefficient with ray angle, Equation (A.12), when the ray angle reaches the Mach

angle of the flow behind the shock wave, the pressure coefficient is the same as that directly behind the shock wave. For region III the pressure coefficient at the Mach angle is not the same as that behind the shock and varies along the ray. For purposes of simplification, it is assumed that the pressure coefficient along the Mach wave bordering region III is the average value found in region II. It is shown in Appendix IV that this pressure coefficient is approximately one-half of the shock wave pressure coefficient. It is this value which is used in the calculations.

Using the same procedure carried out for the determination of the rolling moment coefficient in region II, the rolling moment coefficient for region III turns out to be

$$C_{\mu_{III}} = C_{p_s} \frac{\left(1 - \frac{AR \cdot T}{2} - h'B\right)^2}{4\pi\, AR} \int_0^{\mu} \frac{\cos^{-1}(1 - 2B\tan\alpha)}{S^2} \left[1 - 4 \frac{\left(1 - \frac{AR \cdot T}{2} - h'B\right)\sin\alpha}{3.AR.S} \right] d\alpha \qquad (A.35)$$

Also, the constant pressure rolling moment coefficient is

$$C_{l_{s_{III}}} = C_{p_s} \cdot \frac{\left(1 - \frac{AR \cdot T}{2} - h'B\right)^2}{4 \cdot AR \cdot (\tan \Lambda_{te} + B)} \left[1 - \frac{2\left(1 - \frac{AR \cdot T}{2} - h'B\right)}{3\, AR\, (\tan \Lambda_{te} + B)} \right] \qquad (A.36)$$

Finally, the loss in rolling moment coefficient in region III is

$$C_{l_{L_{III}}} = C_{l_{s_{III}}} - C_{l_{III}} \qquad (A.37)$$

Total Rolling Moment Coefficient.--The losses in rolling moment coefficient were subtracted from the rolling moment coefficient which would occur if there were no outside influences on the wing surface behind the shock wave. For the shock angle, θ, greater than ϕ the area affected by the shock wave is given by

$$A = \frac{b}{2}\left(c - \frac{b \cdot T}{4}\right) \tag{A.38}$$

In non-dimensional form based on the total exposed wing area with no taber, Equation (A.38) becomes

$$A' = \frac{\left(1 - \frac{AR.T}{4}\right)}{2} \tag{A.39}$$

and the moment arm from the root chord to the centroid of the affected area is

$$\bar{y}' = \frac{2(3 - AR.T)}{3(4 - AR.T)} \tag{A.40}$$

The constant pressure rolling moment coefficient is then

$$C_{l_s} = C_{p_s} \cdot \frac{(3 - AR.T)}{12} \tag{A.41}$$

For a shock angle less than ϕ, the area is given by

$$A' = \frac{1}{2\ AR.T} \tag{A.42}$$

The moment arm is

$$\bar{y}' = \frac{2}{3\ AR.T} \tag{A.43}$$

and the rolling moment coefficient for a constant pressure coefficient is

$$C_{l_s} = C_{p_s} \frac{1}{3\,AR^2T^2} \tag{A.44}$$

Finally, the total rolling moment coefficient is given by

$$C_{l_t} = C_{l_s} - \sum C_{l_L} \tag{A.45}$$

where $\sum C_{l_L}$ is the loss in rolling moment coefficient due to three-dimensional effects.

APPENDIX IV

DETERMINATION OF THE AVERAGE PRESSURE COEFFICIENT IN REGION II

The average pressure coefficient is given by

$$C_{p_{avg.}} = \frac{\int_o^{\mu} C_p \cdot dA}{\int_o^{\mu} dA} \qquad (A.46)$$

where dA in region II was given by Equation (A.30) to be

$$dA = \frac{\left(c - \frac{b.T}{2}\right)^2}{2 S^2} d\alpha \qquad (A.47)$$

in which

$$S = \sin\alpha \tan \Lambda_{te} + \cos\alpha$$

The pressure coefficient in a conical field is given by

$$C_p = C_{p_s} \cdot \frac{\cos^{-1}}{\pi} (1 - 2 B \tan\alpha) \qquad (A.48)$$

Substitution of Equations (A.47) and (A.48) into Equation (A.46) yields

$$C_{p_{avg.}} = \frac{C_{p_s}}{2A_a} \int_o^{\mu} \frac{\cos^{-1}(1 - 2B \tan\alpha)}{S^2} \left(c - \frac{b.T}{2}\right)^2 d\alpha \qquad (A.49)$$

where A_a is the area of region II found from Fig. 30 to be

$$A_a = \frac{\left(c - \frac{b.T}{2}\right)^2}{2(\tan \Lambda_{te} + B)} \tag{A.50}$$

For a forty-five degree swept wing with no taper, Equation (A.49) can be approximated by

$$C_{p_{avg.}} = \frac{\left(c - \frac{b.T}{2}\right)^2}{2 A_a} \left[\frac{2 B - 1}{2 \sqrt{(2 B + 1)^2 - 1}} - \frac{B - 1}{2(B + 1)} \right] \tag{A.51}$$

Substitution of Equation (A.50) into (A.51) then yields for a forty-five degree swept wing

$$\frac{C_{p_{avg.}}}{C_{p_s}} = \frac{B + 1}{2} \left[\frac{2B - 1}{\sqrt{(2 B + 1)^2 - 1}} - \frac{B - 1}{B + 1} \right] \tag{A.52}$$

Over the range $1.0 \leq B \leq 3.0$ the average of Equation (A.52) is 0.42. For a rectangular wing Equation (A.49) reduced to

$$C_{p_{avg.}} = \frac{C_{p_s}}{4B A_a} \left(c - \frac{b.T}{2}\right)^2 \tag{A.53}$$

or

$$\frac{C_{p_{avg.}}}{C_{p_s}} = 0.5 \tag{A.54}$$

BIBLIOGRAPHY

1. Stone, David G., Recent Data on Controls, National Advisory Committee for Aeronautics, Research Memorandum No. L 52 A10, 1952.

2. Schult, Eugene D., Free-Flight Investigation at Mach Numbers Between 0.5 and 1.7 of the Zero-Lift Rolling Effectiveness and Drag of Various Surface, Spoiler, and Jet Controls on an 80° Delta-Wing Missile, National Aeronautics and Space Administration, Technical Note No. D-205, 1960.

3. Hunter, Paul A., An Investigation of the Performance of Various Reaction Control Devices, National Aeronautics and Space Administration, Memo. No. 2-11-59L, 1959.

4. Hedgepeth, John M. and Kell, Robert, Jr., Rolling Effectiveness and Aileron Reversal of Rectangular Wing at Supersonic Speeds, National Advisory Committee for Aeronautics, Technical Note No. 3067, 1954, p. 79.

5. Eggers, A. J., Jr., and Syvertson, Clarence A., Aircraft Configurations Developing High Lift-Drag Ratios at High Supersonic Speeds, National Advisory Committee for Aeronautics, Research Memorandum No. A55 L05, 1956.

6. Holder, D. W., and Lock, R. C., "Lateral Control at Supersonic Speeds by Means of Control Surfaces on Nacelles or on the Fuselage", Journal of the Royal Aeronautical Society, Vol. 62, June, 1958, pp. 446-449.

7. Perkins, Courtland D., and Hage, Robert E., Airplane Performance, Stability, and Control, John Wiley and Sons, Inc., New York, 1958, pp. 353-355.

8. Strass, H. Kurt, and Marley, Edward T., Rolling Effectiveness of All-Moveable Wings at Small Angles of Incidence at Mach Numbers from 0.6 to 1.6, National Advisory Committee for Aeronautics, Research Memorandum No. L51 H03, 1951.

9. Sandahl, Carl A., Strass, H. Kurt, and Piland, Robert O., The Rolling Effectiveness of Wing-Tip Ailerons as Determined by Rocket-Powered Test Vehicles and Linear Supersonic Theory, National Advisory Committee for Aeronautics, Research Memorandum No. L50 F21, 1950.

10. Strass, H. Kurt, The Effect of Spanwise Aileron Location on the Rolling Effectiveness of a Wing with 0° and 45° Sweep at Subsonic, Transonic, and Supersonic Speeds, National Advisory Committee for Aeronautics, Research Memorandum No. L50 A27, 1950.

11. Sandahl, Carl A., Free-Flight Investigation at Transonic and Supersonic Speeds of the Rolling Effectiveness of a 42.7° Swept Back Wing having Partial-Span Ailerons, National Advisory Committee for Aeronautics, Research Memorandum No. L8 E25, 1948.

12. Ames Research Staff, Equations, Tables, and Charts for Compressible Flow, National Advisory Committee for Aeronautics, Report No. 1135, 1953.

13. Jacobsen, Carl R., Effects on Control Effectiveness of Systematically Varying the Size and Location of Trailing-Edge Flaps on a 45° Sweptback Wing at a Mach Number of 1.9, National Advisory Committee for Aeronautics, Research Memorandum No. L51 I26, 1951.

14. Conner, D. William, and May, Ellery B., Jr., Control Effectiveness and Hinge-Moment Characteristics of a Tip Control Surface on a Low-Aspect-Ratio Pointed Wing at a Mach Number of 1.9, National Advisory Committee for Aeronautics, Research Memorandum No. L9 H26, 1949.

15. Goin, Kennith L., Investigation at a Mach Number of 1.9 and a Reynolds Number of 2.2×10^6 of Several Flap-Type Lateral-Control Devices on a Wing Having 42.7° Sweepback of the Leading Edge, National Advisory Committee for Aeronautics, Research Memorandum No. L9 A18a, 1949.

16. Jacobsen, Carl R., Control Characteristics of Trailing-Edge Spoilers on Untapered Blunt Trailing-Edge Wings of Aspect Ratio 2.7 with 0° and 45° Sweepback at Mach Numbers of 1.41 and 1.96, National Advisory Committee for Aeronautics, Research Memorandum No. L52 J28, 1952.

17. Busemann, Adolf, Infinitesimal Conical Supersonic Flow, (Translation), National Advisory Committee for Aeronautics, Technical Memorandum No. 1100, 1947.

18. Nielson, Jack N., Missile Aerodynamics, McGraw-Hill Book Co., Inc., New York, 1960, pp. 22-24.